ASSESSING THE MECHANICAL BEHAVIOR OF TREATMENTS FOR FOCAL ARTICULAR CARTILAGE LESIONS

A Dissertation

Presented to the Faculty of the Graduate School

of Cornell University

In Partial Fulfillment of the Requirements for the Degree of

Doctor of Philosophy

by

Darvin Griffin

February 2016

ASSESSING THE MECHANICAL BEHAVIOR OF TREATMENTS FOR FOCAL ARTICULAR CARTILAGE LESIONS

Darvin Griffin, Ph.D.
Cornell University 2016

In a healthy knee joint, articular cartilage (AC) supports loads, dissipates energy, and lubricates with little to no signs of wear or damage. With injury or degeneration related to osteoarthritis (OA), cartilage changes occur leading to significant loss of mechanical function, with the potential to cause further progressive degeneration of cartilage.

While the connection between mechanical changes and arthritis progression is well known, previous work has focused primarily on bulk, tissue-scale (≈1mm) behavior. What is less clear is how mechanical behavior changes on the microscale (e.g. ≈10-20μm) during cartilage degradation. Previous work in our lab has developed techniques for measuring local strains in healthy cartilage via confocal elastography. This work focuses on applying traditional and novel techniques to understand the mechanical behavior at degraded and repaired articular cartilage. The first aim elucidates the fundamental relationships between the composition and structure of degraded cartilage and its local mechanical behavior, specifically its viscoelastic response with degeneration. This study combined state of the art techniques for analyzing cartilage structure, and high resolution mapping of mechanical properties on the microscale(≈20μm). This work provided new insight into structural and local

mechanical changes that occur in cartilage during the early stages of OA. Due to its avascular nature, articular cartilage exhibits an extremely limited capacity to heal when damaged. Consequently, research dealing with cartilage repair strategies is of elevated importance. Restoring the mechanical properties of tissue at the repair site is a common problem in tissue engineering techniques aimed at repairing cartilage defects. Therefore, the second and third aims investigated the mechanical performance of repaired cartilage treated with either matrix membranes or growth factors to assist in tissue formation within a defect site and surrounding AC.

The present work has developed into an innovative mechanical characterization technique. Specifically, combining the confocal elastography technique, with the unique sample populations from second and third aim to tackle a problem that has faced the orthopedic research field for more than two decades: understanding the mechanics of the interface between native and repaired cartilage. I've identified two distinct error modes of failure for this interface – sliding and peeling. As such, understanding the structure function relationship in healthy, damaged, and repaired cartilage, is critical for devising strategies to restore tissue impaired by injury or disease and can provide a template for successful implant design.

BIOGRAPHICAL SKETCH

As one of three male children who is a product of a single parent home from Shuqualak, MS, Darvin knew firsthand the importance of hard work, commitment, and preparation to ensure success. From a young age, Darvin discovered a strong interest in science and mathematics—an interest which later served as a background for his passion in pursuing a career in engineering

Darvin gained a fascination in competing in regional and state science fairs. During his years at Noxubee County High School in Macon, MS, he was awarded "Best of Fair" at regional and statewide fairs, and received 3rd place at the international level. In 2009, he graduated from Mississippi State Univeristy with a Bachelors of Science degree in biological engineering.

Darvin's public impact extends beyond his research as an active mentor to minority students in the Science, Technology, Engineering & Mathematics (STEM) fields at the middle school and college levels. Darvin has personally lead programming and mentored over 230 pre-college Black and Latino high school students in the summer program, CATALYST Academy as the Residence Hall Director. Darvin has assisted them with engaging in engineering research and design projects, college admissions, and general role modeling for these young scholars. His leadership within these outreach events has been particularly influential in efforts to increase undergraduate women and minorities in Cornell Engineering.

Darvin enjoys traveling, reading, outdoor athletic sports, listening to classical musical, engaging in conversation, and going to the gym.

This thesis is dedicated to my loving mother, Ms. Johnnie Mae Griffin.

ACKNOWLEDGMENTS

First, I am grateful to my advisor, Professor Lawrence J. Bonassar, for his mentorship, patience, expertise, and direction. Next, the work in this thesis would not have been possible without the guidance and support of my committee members Professor Itai Cohen and Professor Alan Nixon. I have had the privilege of collaborating with an enormous number of talented scientists and engineers. They include Mark Buckley, Devin Lachowsky, Edward Bonnevie, Natalie Galley, Grace Kim, Derin Sevenler, James Hart, Holly Sparks, Nance Moran, Gloria Matthews, Kyla Ortved, Amanda Meppelink , Mark Randolph, Professor Marjolein van der Meulen, Professor Nelly Farnum. I would also like to thank the following funding sources for the projects described in this thesis: Diversity Programs in Engineering- Cornell University Sage Fellowship, National Science Foundation Graduation Research Fellowship (NSF Grant No. DGE-0707428), SUNY Graduate Diversity Fellowship, Provost Diversity Fellowship. In addition, I would like to acknowledge members of the Bonassar, Cohen, and Biomechanics groups who have provided instrumental advice and assistance throughout the duration of this project including: Olufunmilayo Adebaya, Brandon Borde, Katherine Hudson, Corrine Reid Hanek, Lena Bartell, Michelle Delco, Lisa Fortier.

Finally, I would like to thank my entire family, specifically Travis, Paras, Mom for their support and love.

TABLE OF CONTENTS

LIST OF FIGURES

LIST OF ABBREVIATIONS

AC	articular cartilage
OA	osteoarthritis
PGs	proteoglycans
GAG	glycosaminoglycan
ECM	extracellular matrix
MMP	matrix metalloproteinase
ADAMTS	a disintegrin and metalloproteinase with thrombospondin motifs
ACI	autologous chondrocyte implantation
MACI	matrix-assisted autologous implantation
IGF-I	insulin-like growth factor-I
IL-1	interleukin-1
TNF-α	tumor necrosis factor-alpha
TNF-β	tumor necrosis factor-beta
PBS	phosphate-buffered saline
CRM	confocal reflectance microscopy
GRATE	grid resolution automated tissue elastography
5-DTAF	5-dichlorotriazinyl aminofluorescein
TDIS	tissue deformation imaging stage
ANOVA	analysis of variance
HA	aggregate modulus
IACUC	institutional animal care and use committee
EDTA	ethylenediaminetetraacetic acid
IHC	immunohistochemistry
DSRC	dynamic self-regenerating cartilage

CHAPTER 1

INTRODUCTION

1.2 STRUCTURE AND COMPOSITION OF ARTICULAR CARTILAGE

Cartilage plays an important mechanical role in the functioning of joints. Creating an almost frictionless surface at the bone surface, it absorbs and dissipates the loads that would otherwise be directly experienced by the bones. Cartilage has three main functions that correspond to different components: collagen provides tensile strength; proteoglycan (PG) aggregates provide compressive stiffness; and non-collagenous proteins provide cell-matrix interactions[1]. Articular cartilage (hyaline cartilage) is one of the three main types of cartilage composed of type II collagen. It covers all the diarthroidal joints of the body.

Collagen makes up 60% of the dry weight of cartilage. Collagen forms a macrofibrillar collagen network made of numerous collagen fibrils. These fibrils are nonhomogeneous, and differ in both size and length. They provide tensile stiffness, strength and cohesiveness of cartilage[2]. Type II collagen makes up 90-95%[2] of the total collagen of articular cartilage.

Proteoglycans (PGs) make up 25-25% of the dry weight of cartilage[2]. The basic structure includes a protein core with one or more negatively charged glycosaminoglycan chains (hyaluronic acid, chondroitin sulfate, keratin sulfate, dermatan sulfate) attached to the core. There are two classes of PGs: small PGs and

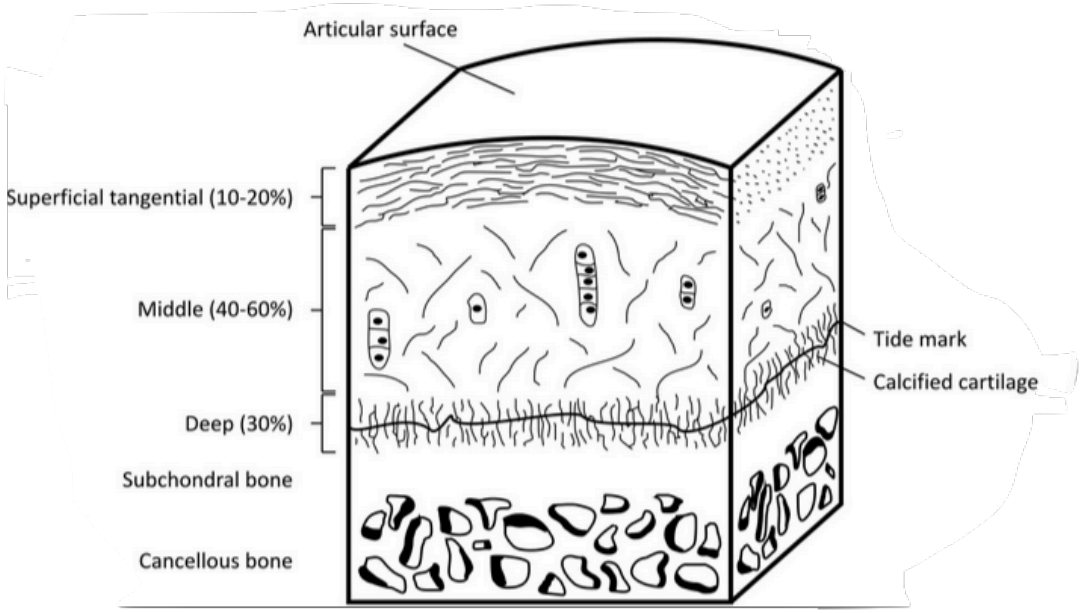

Figure 1.1: Structural layers of articular cartilage.[3]

large aggregating PG monomers (aggrecans). The aggrecans associate with hyaluronic acid and link proteins to form PG aggregates that function to stabilize the PGs in the matrix during deformation and movement[2].

Cartilage is composed of four zones: superficial, middle, deep, and calcified. The superficial zone, the thinnest of the four zones, consist of flat ellipsoid-shaped[2] chondrocytes arranged parallel to the articular surface (Figure 1.1). This zone has the lowest concentration of aggrecan, but the highest concentration of collagen. This high collagen concentration gives the superficial zone the highest tensile properties[1] and is able to resist shear forces. The middle zone has a lower density of cells, lower concentration of water and collagen and higher concentration of aggrecan. The chondrocytes in the middle zone are more rounded; the fibrils have a greater diameter and are randomly oriented. The deep zone has the lowest concentration of cells but the highest concentration of aggrecan. Both the chondrocytes and collagen fibers have a perpendicular orientation.

1.2 FUNCTION OF ARTICULAR CARTILAGE

Articular cartilage serves as a protective layer across diathrodial joints. Cartilage's primary function is transmitting joint loads to the underlying bone under sliding, static, and impact loading. Resultant contact forces in the joints are estimated to be between 2 and 4 times body weight in the knee during walking[4], and up to 18 MPa during rising from a chair[5]. Abnormal joint loading has been linked to the development of osteoarthritis, suggesting that cartilage responds to changes in mechanical loading.

1.3 ARTICULAR CARTILAGE INJURY AND DISEASE

Currently affecting more than 20 million Americans, osteoarthritis (OA) is the second leading cause of physical disability among adults in the United States[6]. OA, also known as degenerative joint disease, involves the deterioration of cartilage in diarthroidal joints that can be attributed to enzymatic digestion and/or various other mechanical alterations of the joint. Acute or severe trauma to the joint may trigger release of cytokines including MMPs, ADAMTS, IL-I, and TNF-α and TNF-β which are all known to alter and erode ECM constituents[7]. Diarthroidal joints are inevitably subjected to repeated stresses that leave cartilage susceptible to mechanical failure; thus, discovering the changes in cartilaginous material properties that normally provide resistance against damage is integral to understanding the progression of this prominent disease. The compromised functionality of cartilage can arise from very subtle changes in the organization of it's structure. As such, observing the effects of damage on the local mechanical properties of cartilage can provide information that may be obscured at the bulk level. Studying how enzymatic digestion affects the unique structure of cartilage will also provide a more comprehensive picture of the intricate relationship between tissue structure and function. Finally, understanding the degradation of cartilage will lead to the development of better biomaterials for cartilaginous tissue replacement or repair.

1.4 ARTICULAR CARTILAGE REPAIR

The loss of articular cartilage due to injury or disease can cause debilitating pain and discomfort. Cartilage is unique in that it does not contain any vascular or neural supply and therefore does

not heal. Since articular cartilage has a poor intrinsic capacity for repair there are two major problems that need to be addressed when attempting to repair articular cartilage. The first is to fill the defect empty space with a tissue that has the same mechanical properties as cartilage and the second is to promote successful integration between the native and repair tissue.

Arguably, the gold standard for cartilage repair is autologous chondrocyte implantation (ACI)[8]. ACI has been in clinical use for cartilage repair for almost three decades now (Figure 1.2a). Chondrocytes are removed from the patient and grown *in vitro* for about six weeks until they reach a 10 to 12 million cell count. After cell proliferation is complete, the patient undergoes another surgery when the chondrocytes are injected into the defect cartilage area. The chondrocytes are held in place by a periosteal flap sutured over the bone[8]. The implanted chondrocytes proliferate and integrate with the surrounding host cartilage to generate hyaline-like cartilage. A study done in 2003 on ACI, showed some formation of hyaline-like cartilage, but mostly the formation of fibrocartilage[9]. However, fibrocartilage does not have the same mechanical properties as hyaline cartilage and is therefore not ideal.

Researchers have begun to evaluate the effects of biomaterials on cartilage repair. Specially, matrix-assisted chondrocyte implantation (MACI®) involves the use of porcine-derived type I/type III collagen bi-layer membrane secured into cartilage defects using fibrin adhesive(Figure 1.2b) [3,9]. MACI® grafts eliminate the need for periosteal harvest, help maintain chondrocyte viability and phenotype, and potentially allows for a more even distribution of cells in the defect[9].

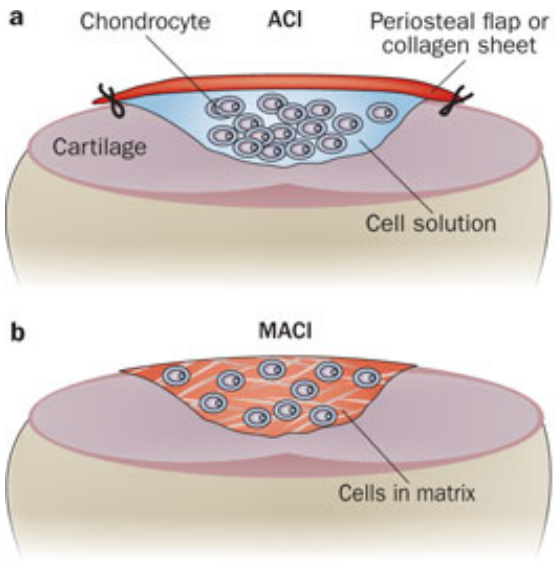

Figure 1.2 Schematic diagram showing **(a)** autologous chondrocyte implantation (ACI) and **(b)** matrix assisted chondrocyte implantation grafts. ACI chondrocytes are inserted into defect and covered with periosteal or collagen sheet. In MACI, isolated and culture-expanded chondrocytes are seeded into a matrix and implanted into defect.[9]

Furthermore, gene therapy has been used to assist in tissue formation within a defect site and surrounding articular cartilage. Specifically, genetically-modified chondrocytes encoding insulin-like growth factor-I (IGF-I) have shown improved arthroscopic and overall repair. rAAV5-IGF-I transfection has been shown to increase aggrecan and type II collagen content in cartilage repair, and improve integration with surrounding cartilage matrix[10,11]. However, the restorative effect of IGF-I on the mechanical properties in a large animal model is poorly understood.

An important outcome parameter for assessing cartilage repair is how well the implant integrates with adjacent host tissue; unfortunately, integrative repair of cartilage does not occur readily in vivo (Figure 1.3). As such, determining the interfacial mechanics of the native and repaired cartilage could shed more light on this problematic in vivo joint defect environment. Thus, an appropriate biomechanical assessment of repair-host tissue retrieved is needed.

1.5 GUIDE TO THE THESIS

This thesis focuses on applying traditional and novel state of the art techniques to understand the mechanical characterization at degraded and repaired cartilage.

Chapter two of my thesis elucidates the fundamental relationships between the composition and structure of degraded cartilage and its local mechanical behavior, specifically its viscoelastic response with degeneration. This study combined state of the art techniques for analyzing cartilage structure, and high resolution mapping of mechanical properties on the microscale (≈20μm).

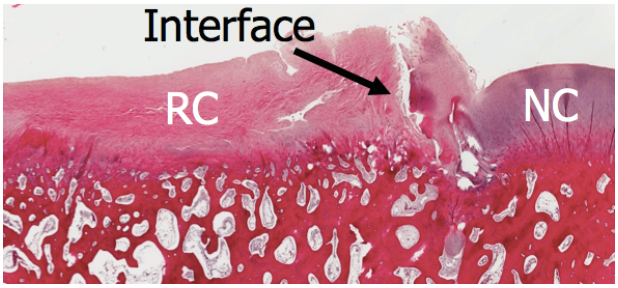

Figure 1.3 Histological cross-section of poor integration of repaired cartilage and native articular cartilage[12].

Due to its avascular nature, articular cartilage exhibits an extremely limited capacity to heal when damaged. Restoring the mechanical properties of tissue at the repair site is a common problem in tissue engineering techniques aimed at repairing cartilage defects. Particularly, there is limited data describing the mechanical performance of engineered cartilage grafts in long term large animal models, which is arguably the most important parameter for predicting the clinical success of grafts. Consequently, the third and fourth chapters investigated the mechanical performance of repaired cartilage treated with either matrix membranes or growth factors to assist in tissue formation within a defect site and surrounding articular cartilage.

Finally, the fifth chapter tackles a problem that has faced the orthopedic research field for more than two decades, which entails understanding the mechanics of the interface of native and repaired cartilage through the use of innovative mechanical techniques.

CHAPTER 2

THE EFFECTS OF ENZYMATIC TREATMENTS ON THE DEPTH-DEPENDENT VISCOELASTIC SHEAR PROPERTIES OF ARTICULAR CARTILAGE[†]

2.1 ABSTRACT

Osteoarthritis (OA) is a disease that involves the erosion and structural weakening of articular cartilage. OA is characterized by the degradation of collagen and proteoglycans in the extracellular matrix (ECM), particularly at the articular surface by proteinases including matrix metalloproteinases (MMPs) and a disintegrin and metalloproteinase with thrombospondin motifs (ADAMTSs) also referred to as aggrecanases[13]. Degradation of collagen and proteoglycans is known to alter shear mechanical properties of cartilage, but study of this phenomenon has been focused on bulk tissue properties. The purpose of this work is to assess microscale cartilage damage induced by trypsin or collagenase using a technique to measure the local shear viscoelastic properties. Safranin-O histology revealed a decrease in proteoglycans near the articular surface after collagenase and trypsin digestions, with proteoglycan depletion increasing over time. Similarly, confocal reflectance micrographs showed increasing collagen degradation in collagenase treated samples, although the collagen network remained

---

[†]Griffin, D., Silverberg, J., Buckley, M., Cohen, I., Bonassar, L. "The effects of enzymatic treatments on the dependent viscoelastic shear properties of articular cartilage," Journal of Orthopedic Research (JOR) 2014, doi: 10.1002/jor.22713.

intact after trypsin treatment. Both treatments induced changes in shear modulus that

were confined to a narrow range (~400μm) near tissue surface. In addition, collagenase altered the total energy dissipation distribution by up to a factor of 100, with longer digestion times corresponding to higher energy dissipation. The ability to detect local mechanical signatures in tissue composition and mechanics is an important tool for understanding the spatially non-uniform changes that occur in articular cartilage diseases such as OA.

2.2 INTRODUCTION

Osteoarthritis involves the deterioration of cartilage in diarthroidal joints that can involve both enzymatic activity and mechanical factors. The compromised functionality of cartilaginous tissues can arise from very subtle changes in the organization of their structure. Furthermore, it has been reported that in OA, structural damage to the collagen and proteoglycan network begins near the cartilage surface before progressing deeper into the tissue[13,14]. Degradation of the ECM by proteinases is known to alter the mechanical behavior of bulk cartilage samples[14], but little is known about the specific changes in material properties near the tissue surface. The lack of knowledge of these changes is in part due to the fact that a reliable method for detecting microscale changes in early OA has not yet been established. As such, observing the effects of damage on the local mechanical properties of cartilage can provide information that may be obscured by measurements at the bulk level.

Previous studies have used degradative enzymes such as matrix metalloproteinase-1 (MMP-1)[15,16,17], MMP-3[18,19] or inflammatory cytokines, including both α and β forms of interleukin-1 (IL-1)[17,18] and TNF-α[18,19] to selectively examine

the effect of proteoglycan and collagen degradation on the mechanical properties of cartilage explants. While these studies demonstrated decreases in tensile[20,21], compressive[22,23] , and shear stiffness[24], the analyses were limited to bulk mechanical behavior. In contrast little is known about local mechanical changes (on the scale of <100μm) that occur in cartilage that has been degraded. Recently, our lab has developed a novel system for measuring the local dynamic shear properties of articular cartilage on the length scale of 20μm[25]. This technique revealed that a narrow region of the tissue 100-200 μm below the articular surface has remarkably different properties than the rest of the tissue[26,27]. This surface region is also damaged or degraded early in the process of arthritis[27]. However the consequences of damage to this region on shear mechanical behavior are not well understood. The purpose of this study was to assess the effect of progressive proteoglycan and collagen degradation induced by trypsin and collagenase on the spatially localized shear properties of cartilage. Understanding the degradation of cartilage locally will provide a more comprehensive picture of the intricate relationship between tissue structure and properties as well as providing insight into the mechanical changes that occur very early upon surface damage.

2.3 MATERIALS AND METHODS

2.3.1 Tissue Sample Preparation

56 full thickness, 6 mm diameter explants were harvested sterilely from the patellofemoral groove of seven 1-3 day old calves (Gold Medal Packing, Oriskany, NY) with samples from each animal randomly assigned between control and

experimental groups (Figure 2.1A). The harvesting procedure produces cylinders with an undamaged articular surface[28]. After dissection, 56 samples were soaked in phosphate-buffered saline (PBS) supplemented with 100 U/mL penicillin and 100 mg/mL streptomycin for 30 minutes. Each cylinder was then cut along its long axis into two hemi-cylinders yielding a total of 112 hemi-cylinders (Figure 2.1B). A small section (1-3 mm) of the deep region of each hemi-cylinder was removed with a razor blade to flatten the facet opposing the articular surface.

2.3.2 Enzymatic Digestion and Confocal Reflectance (CR) Microscopy

Cartilage samples designated for enzymatic digestion and CR imaging of collagen were coated with epoxy resin (Devcon, Danvers, MA) to ensure that enzyme exposure occurred only at the articular surface (Fig. 2.1C). CR microscopy was used to obtain real-time images of cartilage samples without the need for histologic stains[29], where the fluorescence signal intensity is proportional to collagen density. A total of 8 samples were imaged on a confocal reflectance microscope (Zeiss 710 Confocal, Germany) at 25x magnification in real-time at a frame rate of 4 frames/min.

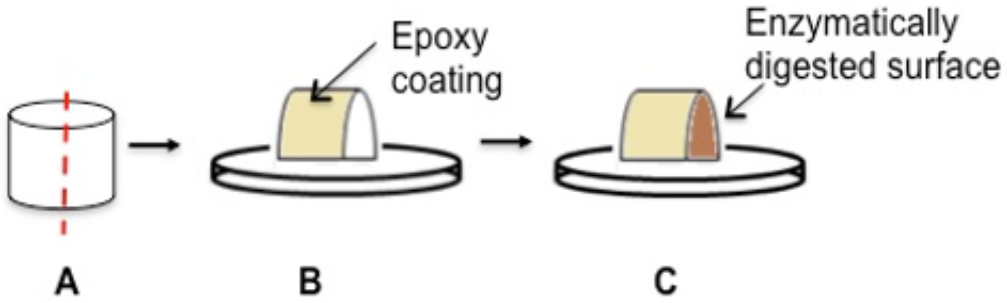

Figure 2.1. (A) 6 mm cylinders are bisected into hemi cylinders (B) coated with epoxy resin (C) 50 μg/mL trypsin or 2 mg/mL collagenase are added to the tissue surface for 15, 30, and 90 minutes.

Samples were digested for 15, 30, and 90 minutes using two different enzymes, 2mg/mL of bacterial collagenase to remove both collagen and proteoglycans (Worthington, type II collagenase, Lakewood, NJ) or 50 μg/mL of trypsin (Cellgro, 0.25% trypsin EDTA, Manassas, VA), which selectively cleaves the core proteins in proteoglycans without affecting the collagen network[16]. During degradation samples were imaged serially at 0, 15, 30, and 90 minutes with 4 samples observed for collagenase or trypsin exposure. After degradation, solutions were removed by serial washing with protease inhibitors in PBS. Additionally, 40 samples were fixed, embedded, sectioned, and stained with Safranin-O to observe proteoglycan distribution after 0, 15, 30, and 90 minutes of exposure to collagenase (n=6 at each time point) or trypsin (n=4 at each time point). In parallel, 44 samples were used for confocal strain mapping studies, with n=7 samples at each time point of collagenase treatment and n=6 samples at each time point of trypsin treatment.

2.3.3 Confocal Strain Mapping

The local shear modulus of samples was measured using grid resolution automated tissue elastography (GRATE) as described previously[28]. Samples were placed in PBS with 200 μL/mL 5-dichlorotriazinyl aminofluorescein (5-DTAF) (Molecular Probes®, Grand Island, NY) for two hours (Fig. 2A)[30,31]. 5-DTAF modifies amines in proteins and fully stains the extracellular matrix. The deep zone of the hemi-cylinders were glued to a tissue deformation imaging stage (TDIS) and compressed to 10% axial strain. The TDIS was mounted on an inverted Zeiss LSM 5 LIVE confocal microscope and imaged using a 488 nm laser (Fig. 2B). To directly image applied strain, a line

perpendicular to the articular surface was photobleached with the confocal laser. Sinusoidal shear displacements were applied to the articular surface by the TDIS at a frequency of 0.1 Hz and amplitude of 16 μm, and the resultant forces were measured with a load cell (Fig.2C).

Custom software written in Matlab (The Mathworks, Inc., Natick, MA) was used to track the motion of the photobleached line as a function of depth[25]. These local displacements were fit to a sinusoidal function and differentiated with respect to z to calculate the strain amplitude $\gamma_0(z)$ and phase angle relative to the resultant stress $\delta(z)$. The shear modulus magnitude |G*(z)| was calculated as the ratio of stress amplitude τ_0 to strain amplitude γ_0, where τ_0 is the total applied stress required to deform the tissue from zero strain to γ_0. The rate of energy dissipation per unit volume at a depth z was calculated by the following equation:

$$\frac{\Delta E}{\Delta v} = \pi \gamma_0^{\,2} |G^*(z)|^{-1} \sin\delta(z)$$

2.3.4 Statistical Analysis

Two-way ANOVA was used to evaluate the statistical significance of enzymatic treatments on the depth-dependent viscoelastic shear properties of articular cartilage.

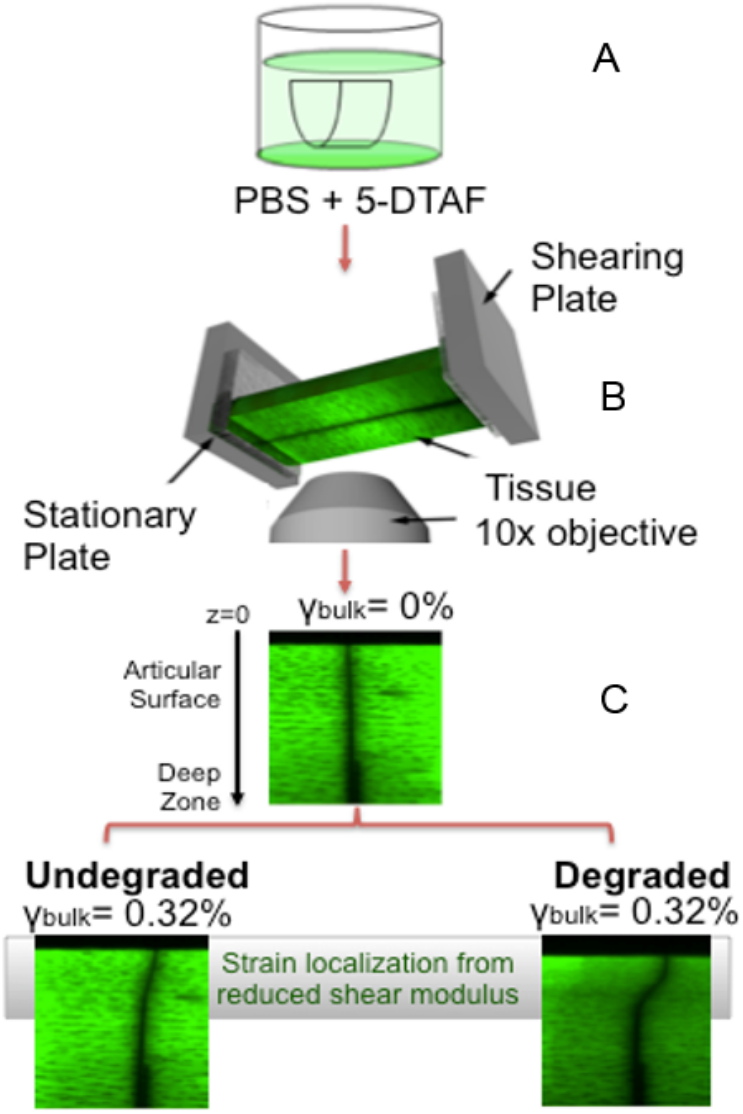

Figure 2.2 (A) Samples were placed in a 200µL of 5-DTAF solution to fluorescently stain the ECM, (B) Schematic of the tissue deformation imaging stage; (C) A line was photobleached perpendicular to articular surface and subjected to 0.32 shear strain before and after digestion. The photobleached line for the degraded specimen exhibited a steeper slope from strain localization, implying inferior surface properties.

2.4 RESULTS

2.4.1 Enzymatic Digestion and Confocal Reflectance (CR) Microscopy

Safranin-O staining revealed a progressive removal of proteoglycans near the articular surface after collagenase digestion with the depth of proteoglycan depletion increasing with time (Fig. 3A-D). Similarly confocal reflectance microscopy revealed degradation of the collagen network with a sharp border between degraded and undegraded regions (Fig. 3E-H). The depth of matrix removed increased from 150 μm at 15 minutes, 300 μm at 30 minutes, and 450 μm at 90 minutes. The depth of proteoglycan and collagen removal was similar at all times (Fig. 3I).

In contrast to collagenase, trypsin removed only proteoglycans (Fig. 4A-D) but not collagen (Fig. 4E-H). The depth of proteoglycan removal progressed from 100μm at 15 minutes, 150 μm at 30 minutes, and 200 μm at 90 minutes (Fig. 4I). Confocal reflectance showed little to no change after trypsin treatment.

2.4.2 Confocal Strain Mapping

As previously reported shear modulus $|G^*|$ for healthy undigested samples exhibited a distinct spatial pattern[24,25,26,30,31](Fig. 5A). The shear modulus was low in a narrow band (~400 μm) near the articular surface, with a well-defined minimum at ~100 μm. Beyond 500 μm in depth the shear modulus showed less variation. Collagenase treatment dramatically lowered the shear modulus at the surface. By 30 minutes $|G^*|$ at 50 μm was reduced by 20% relative to control, and by 90 minutes had decreased by more than 50-fold. The mechanical effect of degradation was confined to 350 μm at 15 minutes, 420 μm at 30 minutes, and 500 μm at 90 minutes. Notably the characteristic minimum $|G^*|$ was not present after 90 minutes of collagenase exposure

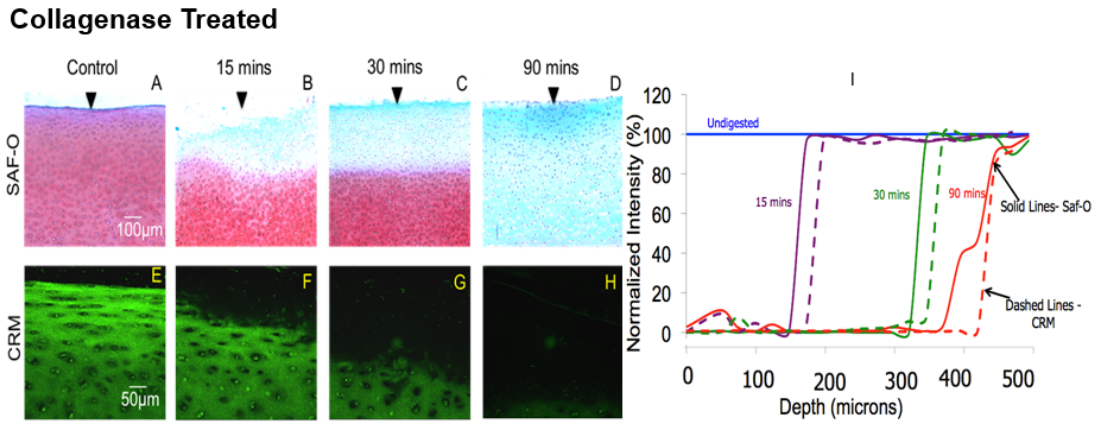

Figure 2.3 (A-D) Saf-O histology and (E-H) confocal reflectance micrographs of articular cartilage before digestion and after 15, 30, and 90 minutes of digestion with collagenase, (I) normalized intensity curves as a function of depth for SAF-O and CRM values (n=6 at each time point).

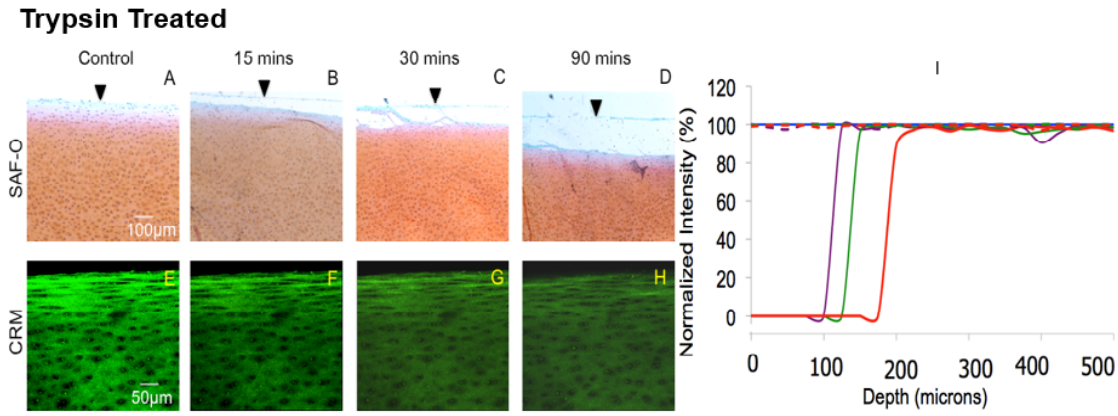

Figure 2.4 (A-D) Saf-O histology and (E-H) confocal reflectance micrographs of articular cartilage before digestion and after 15, 30, and 90 minutes of digestion with trypsin, (I) normalized intensity curves as a function of depth for SAF-O and CRM values (n=4 at each time point).

(Fig. 5A). Collagenase treatment made the tissue more compliant and more viscous at the articular surface leading to an increase in both the local phase angle and local energy dissipation. By 15 minutes both δ and ΔE 90 minutes, were higher than control tissue at depths up to ~500 μm. (Fig. 5B,C).

Similarly to collagenase, trypsin treatment samples displayed similar reduction in $|G^*|$ within the first 400 μm near the articular surface (Fig. 5D). The spatial pattern of change in $|G^*|$ was different between collagenase and trypsin. Trypsin-treated samples had the lowest $|G^*|$ at $z \approx 100$ μm from surface even after 90 minutes of exposure, similar to undegraded tissue (Fig. 5D). This is likely related to the fact that trypsin leaves the collagen network largely intact, as indicated by CRM data. The local phase angle after proteoglycan removal alone increased δ up to 2-fold locally in higher and longer exposure times. A similar mechanical trend was seen with ΔE, by 15mins displaying higher energy dissipation with longer trypsin exposure times.

2.5 DISCUSSION

This study evaluated the effect of progressive proteoglycan and collagen degradation on the depth-dependent viscoelastic shear properties of articular cartilage. In these experiments, enzymatic digestion by trypsin and collagenase at the surface resulted in local structural changes along with a significant reduction in the magnitude of the local shear modulus and a corresponding increase in the energy dissipation and localization. Safranin-O staining revealed a decrease in proteoglycan concentration near the articular surface after either trypsin or collagenase treatment, with

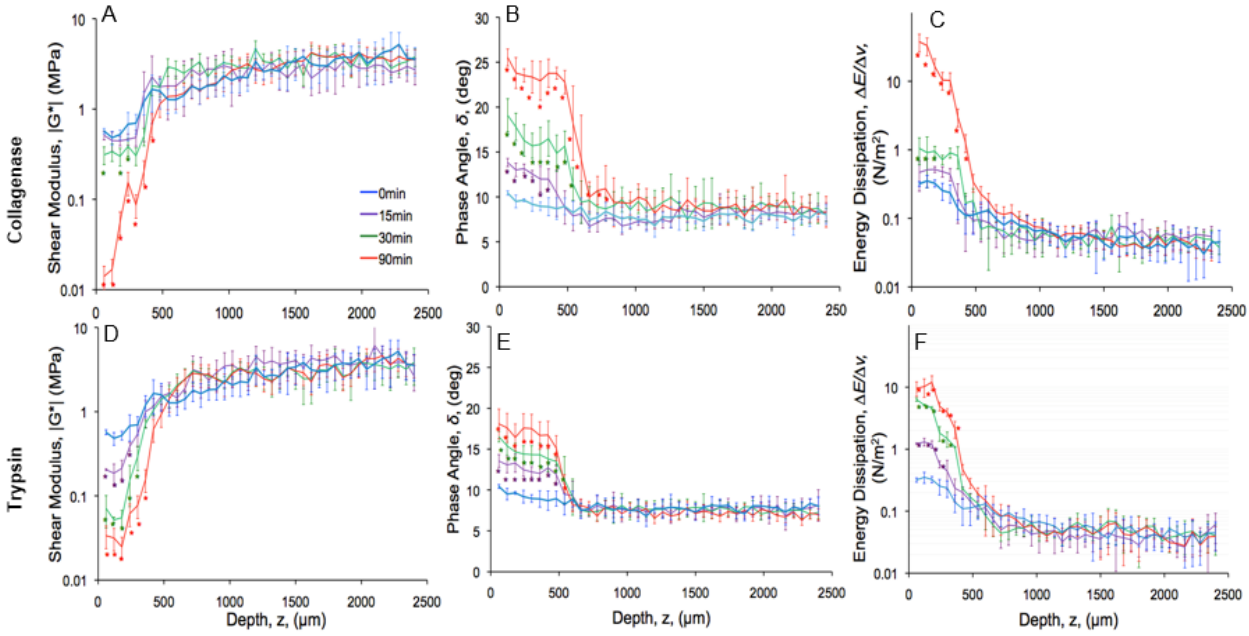

Figure 2.5 (A, B) Shear modulus G) vs. depth z from the surface (C, D) Phase angle (δ) vs. depth z (E,F) Energy dissipated (ΔE) vs. depth z (control n=5, collagenase n=7, and trypsin n=6).

proteoglycan depletion increasing with time. Enzymatic treatments decreased the local shear modulus up to 50-fold, but increased tissue viscoelastic phase lag by up to 2-fold locally, and energy dissipation by up to 100-fold locally (Fig. 5). Because our measurement resolution was 20 μm, we were able to detect such mechanical changes in the tissue near the articular surface where enzymatic degradation occurred.

Histologic examination (Fig. 3,4) showed that the initial loss of proteoglycans and collagen were primarily near the articular surface and progressed deeper into the tissue with time. This progressive front of matrix removal by trypsin[32] and collagenase[33] has been previously documented. Confocal reflectance microscopy produced clear images of the collagen network near the articular surface and similarly, showed a progressive removal after collagenase exposure. In contrast, attenuation of confocal reflectance was associated with trypsin treatment; however, the collagen network appeared intact (Fig. 4E-H). As noted previously[34] collagen removal appeared to also cause proteoglycan removal, as evidence by the fact that collagenase treatment produced fronts that were co-located to within ≈25 μm.

To assess the mechanical consequences of this degradation, we used confocal strain mapping to characterize the viscoelastic shear properties of the tissue. To extend our previous work [24,25,30,31], this study investigated how removal of collagen and proteoglycans affects the mechanical properties in this surface region. Collagenase and trypsin treatments altered the shear modulus $|G^*|$ differently. Collagenase lowered $|G^*|$ dramatically at the surface (Fig. 5A). After 30min of digestion, $|G^*|$ at 20 μm dropped by 30% at the surface, but by 90min, $|G^*|$ surface had dropped so much that there was no visible minimum. In contrast, trypsin treatment lowered $|G^*|$ near

surface, but the $|G^*|$ minimum was always at 100 μm, even after this region had been depleted fully of proteoglycans (Fig. 4D). These data suggest both collagen and proteoglycans contribute to shear properties, but both play a distinct role on bearing shear loads at the articular surface. Particularly, proteoglycan removal lowers the overall magnitude of |G*| and increases the corresponding δ, but preserves the underlying microstructure that produces the characteristic minimum near the surface. Conversely, collagenase digestion, which is a harsher enzymatic treatment of the tissue, affects |G*| and δ the same way as trypsin but also destroys the microstructure that produces the characteristic minimum of |G*| near the surface.

We note this strongly non-linear drop-off in |G*| arising from collagenase digestion (Fig 4A) is consistent with predictions of network-based models of crosslinked polymers[35-39]. In these models, a fibrous network's shear modulus is extremely sensitive to connectivity near the rigidity percolation phase transition. Above the percolation threshold, the crosslinked network is sufficiently connected that stresses can be transmitted through the system. Below the percolation threshold, the network is too fragmented, hence the system is unable to bears stresses and the shear modulus drops dramatically. The data can therefore be interpreted as an enzymatically driven transition that decreases connectivity in the collagen fiber network, and moves the system as a whole toward the percolation phase transition. The data also suggests the proteoglycan network effectively behaves as a simple viscoelastic medium that makes a contribution to |G*| in parallel to the collagen network. Indeed, the observations presented here are consistent with other data that explored these models in greater detail[40].

The local viscoelastic capacity of cartilage under shear has received little attention despite the fact that shear forces in articular cartilage correlate with tissue damage and disease[35]. In cartilage, the osmotic pressure exerted by the proteoglycans keeps the collagen network prestressed with tensile forces[36]. Furthermore, previous studies have shown that cartilage stiffens and becomes less viscous locally when deformed in shear[30]. Both of these studies therefore suggest that stressed or extended collagen networks are more elastic and less viscous, implying that removing such stress would make the network more compliant and more viscous. In the current study, specific removal of proteoglycans by trypsin treatment removed prestress chemically, making the tissue more compliant and more viscous at the articular surface leading to a very large local energy dissipation (Fig. 5F). Previous work reports that articular cartilage dissipates shear energy primarily near its surface[25]. The results of this study suggest that cartilage degeneration compromises this energy-absorbing surface region, therefore increasing tissue susceptibility to shear-induced damage into the remainder of the tissue.

Proteoglycan removal increased viscous behavior, which runs counter to the idea that proteoglycan-proteoglycan friction or collagen-proteoglycan friction is responsible for this viscous behavior. The combination of proteoglycan and collagen removal increased viscous behavior more than proteoglycan removal alone implying the removal of tension on the collagen network contributes to increased viscous behavior. Collagenase increased the rate of energy dissipation by cartilage up to 100-fold locally progressing higher at longer exposure times (Fig. 5C).

The mechanical effect of enzymatic digestion to the cartilage matrix was seen

at depths beyond areas where histological staining was lost (~400 μm). Local proteoglycan and collagen removal by collagenase decreased $|G^*|$ up to ~500μm with increasing mechanical effects in δ and ΔE. Histology indicated initial loss of proteoglycans only up to ~200μm for trypsin-treated samples(Fig.4D); however mechanical reductions were seen up to ~500 μm in $|G^*|$, with increasing values in δ, and ΔE that extended beyond the boundary of degraded tissue. This suggest that local mechanical measurements are a sensitive measure of changes in cartilage shear properties because they can resolve changes in depth-wise variations as well as differences in the overall magnitude. This provides an attractive complement to histological imaging, which offers more explicit static structural information, and can be used in a synergistic fashion to develop a more robust understanding of healthy and disease tissue integrity.

Overall, our results provide novel information on cartilage mechanics and insights on the mechanisms for changes in matrix composition and functional properties associated with matrix degradation. As in early stages of OA, these treatments cause local superficial matrix damage, with concomitant reductions of surface mechanical properties on the microscale. Collectively this data provides a distinct role for collagen and proteoglycans in bearing shear loads at the articular surface. This may be of particular importance, given that depletion of these ECM constituents is known to occur in early osteoarthritis.

2.6 ACKNOWLEDGEMENTS

The authors gratefully acknowledge Olufunmilayo Adebayo, Brandon Borde, and Eddie Bonnie for their helpful discussions and suggestions. This work was supported by Cornell University, NIH R21AR054867, NIH NIAMS 3R01AR053571-0351, and the National Science Foundation Graduate Research Fellowship.

CHAPTER 3

MECHANICAL CHARACTERIZATION OF MATRIX-INDUCED AUTOLOGOUS CHONDROCYTE IMPLANTATION (MACI®) GRAFTS IN AN EQUINE MODEL AT 53 WEEKS‡

3.1 ABSTRACT

There has been much interest in using autologous chondrocytes in combination with scaffold materials to aid in cartilage repair. In the present study, a total of 27 animals were used to compare the performance of matrix-assisted chondrocyte implantation (MACI®) using a collagen sponge as a chondrocyte delivery vehicle, the sponge membrane alone, and empty controls. A total of three distinct types of mechanical analyses were performed on repaired cartilage harvested from horses after 53 weeks of implantation: 1) compressive behavior of samples to measure aggregate modulus (HA) and hydraulic permeability (k) in confined compression; 2) local and global shear modulus using confocal strain mapping; and 3) boundary friction coefficient using a custom-built tribometer. Cartilage defects receiving MACI® implants had equilibrium modulus values that were 70% of normal cartilage, and were not statistically different than normal tissue. Defects filled with MaixTM membrane

---

‡Griffin, D., Lachowsky, D., Bonnevie, E., Hart, J., Sparks, H., Cohen, I., Nixon, A., Moran, N.(Genzyme), Matthews, G.(Genzyme), Bonassar, L. "Mechanical performance of the matrix-induced autologous chondrocyte implant(MACI®) grafts in an equine model at 53 weeks," Journal of Biomechanics (JBM) 2014, doi:10.1016/j.jbiomech.2015.04.010.

alone or left empty were only 46% and 51%-63% of control, respectively. The shear modulus of tissue from all groups of cartilage defects was between 4 to 10 times lower than control tissue, and range from 0.2 to 0.4 MPa. The average values of boundary mode friction coefficients of control tissue from all groups ranged from 0.42 to 0.52. This study represents an extensive characterization of the mechanical performance of the MACI® implant in a large animal model at 53 weeks. Collectively, these data demonstrate a range of implant performance, revealing similar compressive and frictional properties to native tissue, with inferior shear properties.

3.2 INTRODUCTION

Articular cartilage has limited ability for self-repair, and as such any defects leave the affected joint susceptible to osteoarthritis[41]. Both autologous chondrocyte implantation (ACI) and matrix induced autologous chondrocyte implantation (MACI®) have been shown to effectively repair full-thickness chondral defects as evidenced by histology and integration[41-44].

Despite the widespread clinical use of such techniques, there is relatively little known about the mechanical properties of the tissue that results from the use of different cartilage repair techniques. Several studies report compressive properties obtained through indentation [45,46,] unconfined [47], and confined compression tests [48,49]. Confined compression testing on ACI repaired equine tissue showed an aggregate modulus that was only 12% of native tissue [48]. A MACI graft with a type II collagen membrane was shown to have an aggregate modulus that was 15% of native tissue [50].

Stiffness tests in a ovine model showed that MACI® grafts ranged from 16-50% of native cartilage, respectively [51,52]. The duration of implanted tissue ranged from as short as a few weeks to as long as several years. A general trend shown in this data is that longer implant durations tend to perform better, indicating that mechanical properties of repaired cartilage may improve over time.

The current study was motivated by the lack of data on other critical mechanical properties of autologous chondrocyte grafts. For example, there are no published papers that study friction or shear properties of the repaired cartilage in long-term large animal models. In this study, we performed an array of mechanical tests to more fully understand the functionality and mechanical behavior of matrix-induced autologous chondrocyte implanted defects. Therefore, the primary objective of this study was to characterize the compressive, shear, and friction properties of MACI implant repaired articular cartilage after 53 weeks in an equine model.

3.3 MATERIALS AND METHODS

3.3.1 Chondrocyte isolation and expansion

Cartilage biopsies were obtained arthroscopically from the femoral trochlear ridge of 24 horses. Cartilage samples were enzymatically digested and expanded in vitro before seeding on sterile processed collagen type I/III membranes (ACI-Maix™; Genzyme Corporation). Cells were seeded at 0.5 million chondrocytes per cm^2 of collagen membrane, and covered with DMEM and incubated for 48 hours before implantation. Additionally, a collagen type I/III membrane was cultured without

chondrocytes, for use in control defects implanted with membrane alone.

3.3.2 Implantation Surgery

A total of 27 skeletally mature horses (1.5-6 years of age, 300-400 kg weight) free of lameness were used. Arthrotomy surgeries were performed according to the guidelines of the Institutional Animal Care and Use Committee (IACUC) at Cornell University. Two full-thickness chondral defects (15 mm diameter) were created on the femoral trochlear ridge of one hind limb of each horse, using a trephine and cannula. These lesions extended down to, but not through, the subchondral bone plate, and resulted in minimal bleeding or seepage of marrow into the defect. Specifically, defects were placed in both the proximal and distal region of the trochlea in either the right or left joint, with the contralateral joint left unoperated for control (Figure 1). Animals were assigned to one of three cohorts based on treatment provided in each of the two defects: 1.) MACI® graft in one defect and the carrier scaffold, consisting of the ACI-Maix (Matricel) membrane without the presence of cells in other defect (n=12); 2.) MACI® graft and an empty defect (n=12); and 3.) Both defect sites left empty (n=3). The choice of operation on the right or left joint along as well as location within the trochlea was randomized, with all subsequent histological and mechanical analysis performed in a blinded fashion. After 53 weeks, the horses were euthanized and samples were immediately harvested for histological examination and mechanical assessment (Figure 3.1).

3.3.3 Histology and Immunohistochemistry

Samples were decalcified in ethylenediaminetetraacetic acid (EDTA) and

sectioned at 6microns, as previously described [53]. Sections were stained with H&E for morphology and toluidine blue for histochemical reaction to cartilage GAG moieties. Serial sections were used for positive and negative reactions for collagen type II immunohistochemistry [13].

3.3.4 Confined Compression

A total of 108 full thickness cylindrical plugs (3 mm diameter) were harvested from the defect region using a biopsy punch perpendicular to the articular surface. The plugs were thawed in a bath of phosphate buffer saline (PBS) containing protease inhibitors. This procedure was repeated for samples harvested from the proximal and distal region of the trochlea in the control joint. Prior to testing, sample heights were measured using a caliper. Samples were placed in a 3 mm confining chamber, covered

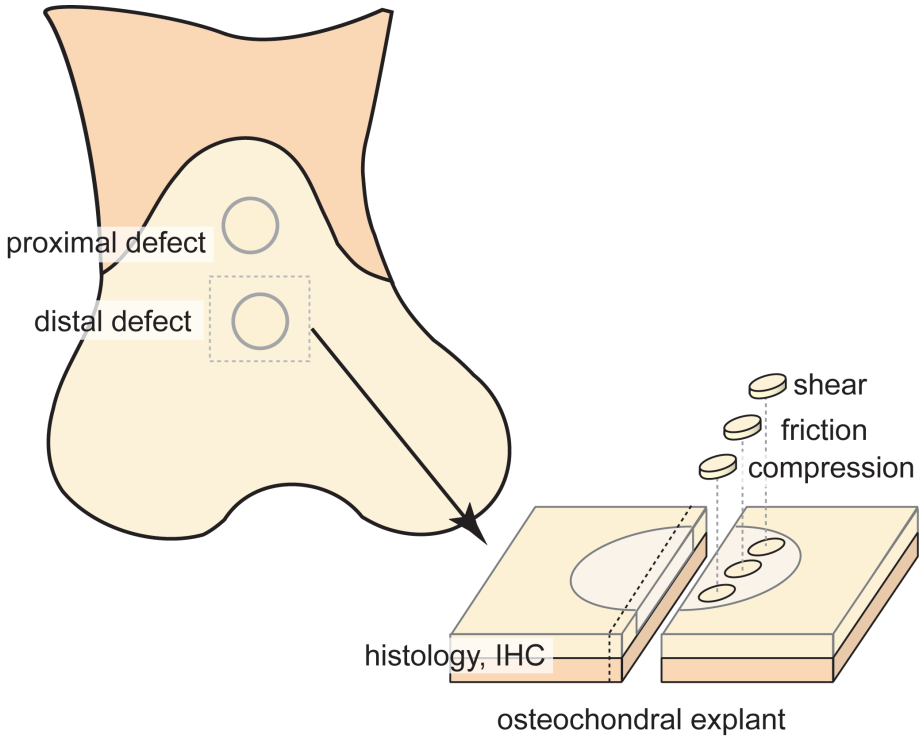

Figure 3.1 Two 15 mm defects are placed into the trochlea of the right or left limb of each horse and either left empty, or filled with MAIX membrane or MACI graft. Osteochondral blocks were extracted after sacrifice with sections taken for histology containing both repair and local tissue and 3 mm plugs taken for each of shear, friction, and compression testing.

with a porous plug and PBS with protease inhibitors, and mounted in a Bose EnduraTEC ELF 3200 for stress-relaxation testing. A series of 5% steps in compressive strain were imposed on each sample up to a total of 40% strain. For each step, the resultant load was measured for 10 minutes using a Honeywell 50lb load cell at a frequency of 1 Hz. The stress-relaxation curves were fit to a poroelastic model and analyzed using custom MATLAB code to calculate aggregate modulus (Ha) and hydraulic permeability (k) [54], [55].

3.3.5 Friction Testing

A total of 84 full thickness cylindrical plugs (3 mm diameter) were tested in a custom tribometer to measure boundary friction coefficients as previously described [56, 54, 57, 58]. Samples were linearly reciprocated against glass at a speed of 0.1 mm/s under 40% strain while bathed in PBS, conditions known to induce boundary mode lubrication. During sliding, both normal and shear forces were collected to determine the friction coefficient. The friction coefficient was calculated by averaging shear force divided by normal force, for both directions of sliding.

3.3.6 Shear Confocal Strain Mapping

A total of 84 full thickness cylindrical plugs (3 mm diameter) were prepared for confocal strain mapping as described previously [59, 60, 61, 62, 63]. Samples were bisected longitudinally into hemi-cylinders, exposed to 7 μg/mL 5-dichlorotriazinyl-aminofluorescein (5-DTAF) for 2 hours to uniformly stain the extracellular matrix,

and rinsed in PBS for 30 minutes. Briefly, samples were glued to a tissue deformation imaging stage (TDIS) and compressed to 10% strain. The TDIS was mounted on an inverted Zeiss LSM 510 5 Live confocal microscope and imaged using a 488 nm laser. A line perpendicular to the articular surface was photobleached using the laser at full intensity. Sinusoidal shear displacements were placed on the articular surface by the TDIS at a frequency of 0.1 Hz and amplitude of 16μm, and the resultant forces were measured with a load cell. Simultaneously, images of the sample deforming were collected at 10 frames per second. Using custom MATLAB code, the intensity minima corresponding to the location of the photobleached line was tracked, and the local strains were determined from the slopes of that line. The local shear modulus (G) was calculated from the local strain and measured load.

3.3.7 Statistical Analysis

For the confined compression tests, each defect was matched to a contralateral control in the opposite joint. Comparison between repair groups and corresponding contralateral controls was performed using a two-tailed paired t-test with bonferroni correction. Minimum detectable differences between control and repaired cartilage were calculated based on sample size, the standard deviation of repaired cartilage, and assuming a power of 0.8. For both friction and confocal strain mapping, it was not possible to harvest a defect sample from every joint. Therefore, a standard two-tailed t-test assuming unequal sample variance between groups was used to analyze the repair groups to control. For all mechanical tests, a one-way analysis of variance (ANOVA) test was performed between all testing groups. Finally, the MACI® group

and empty group were compared using a two-tailed t-test. All data groups are displayed as mean values with standard deviations noted by error bars. Differences were considered significant for $p < 0.05$.

3.4 RESULTS

3.4.1 Histology and Immunohistochemistry

H&E stain revealed improved filling and attachment of MACI® implants compared to cell free ACI-Maix implants and spontaneous healing in the empty defect (Figure 3.2). Toluidine blue reactive cartilage was thicker in MACI® implanted defects, compared to Maix or empty defects. Similarly, collagen type II was more abundant in MACI® implanted defects, compared to empty defects.

3.4.2 Confined Compression

Cartilage from defects receiving MACI® implants had an equilibrium modulus that was 70% of normal cartilage, which was not statistically different than native control tissue ($p=0.07$) (Figure 3.3A). Based on power calculations, the minimum detectable difference between groups was 0.23MPa which was lower than the

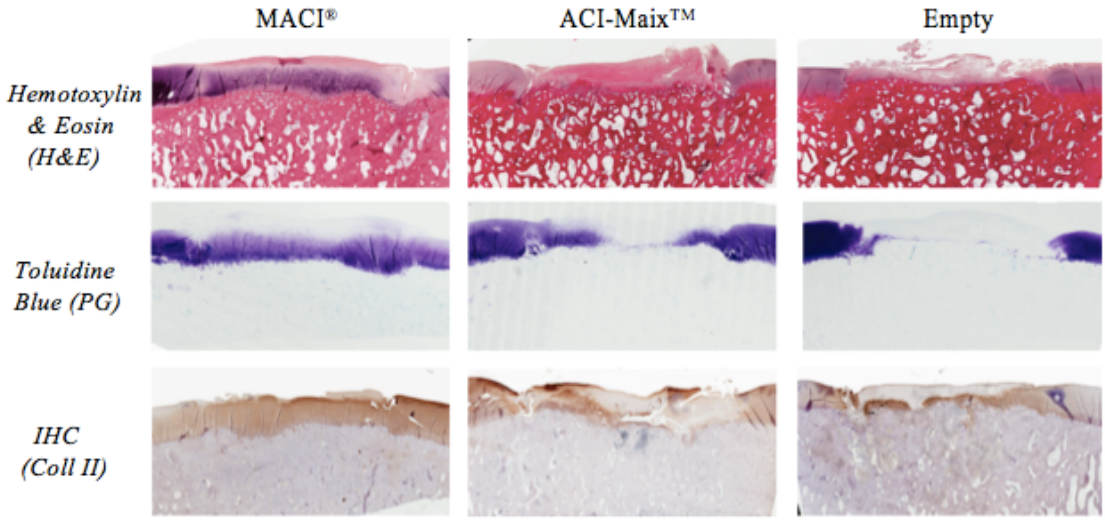

Figure 3.2 Histological and immunohistochemical photomicrographs of MACI®, ACI-Maix (cell-free), and empty implanted defects 53 weeks after repair.

difference between the MACI® and control moduli (0.31MPa). Defects filled with ACI-Maix™ membrane alone or left empty had equilibrium moduli that were 46% ($p<0.05$) and 59% ($p<0.05$) of control, respectively. The hydraulic permeability of tissue from MACI® grafts were 2.6 – 7.0 times higher than control tissue, but were not statistically different from control (Figure 3.3B). Hydraulic permeability of groups with ACI-Maix™ membrane alone were 2.5 times higher than control, but were less varied, and as a result were statistically different from controls. Empty defects had 2.3 to 6.6 times higher hydraulic permeability values than controls, with only one group statistically different.

3.4.3 Coefficient of Friction

The average values of boundary mode friction coefficients of control tissue and from all implant groups ranged from 0.42 to 0.52 with no statistical difference between groups (Figure 3.4A).

3.4.4 Confocal Strain Mapping

The global values of shear modulus for control cartilage ranged from 1.0 -1.5 MPa, consistent with previous data [59, 60, 61, 62, 63] (Figure 3.4B). The shear moduli of tissue from all groups of cartilage defects were four to ten times lower than control cartilage, and ranged between 0.2 to 0.5 MPa. ($p<0.05$)

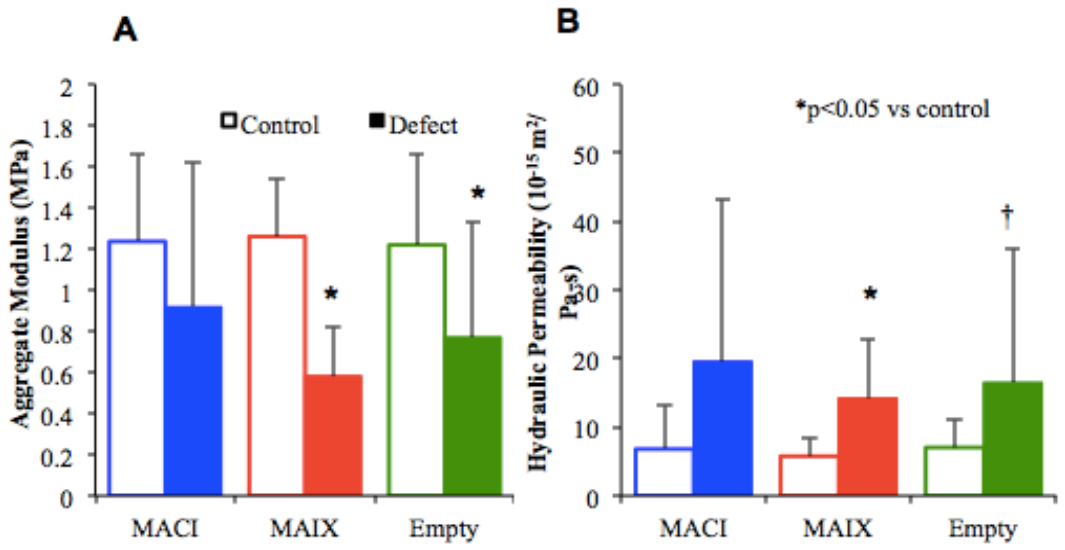

Figure 3.3 Average **A)** aggregate modulus and **B)** hydraulic permeability for each group and its contralateral control. All values expressed as mean ± standard deviation (n=12 for groups MACI and MAIX, n=6 for group Empty). *p<0.05 vs. native control tissue, † one group statistically different.

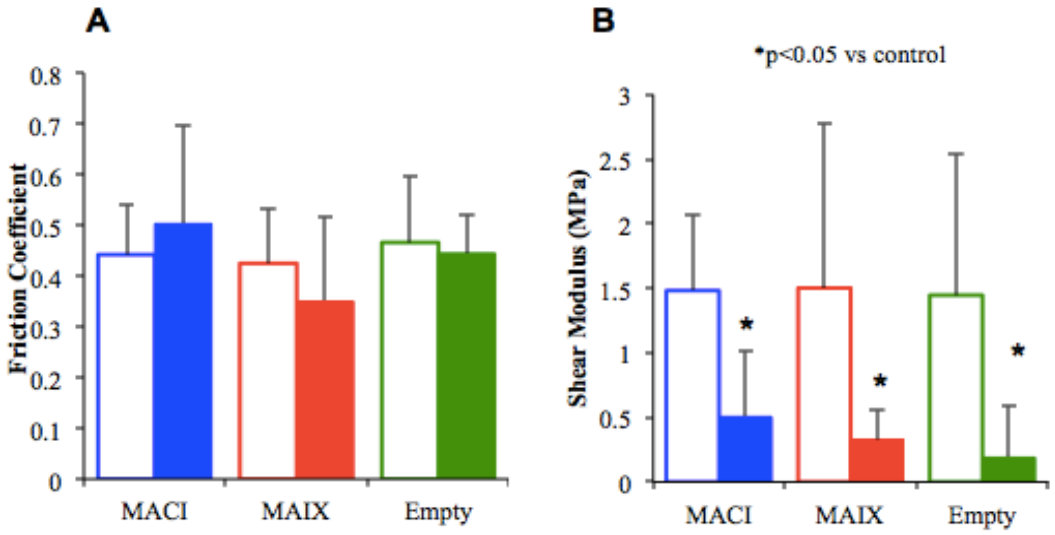

Figure 3.4 Average **A)** boundary mode friction coefficients **B)** global shear modulus for each group and its contralateral control. All values expressed as mean ± standard deviation (n=12 for control groups MACI & MAIX, n=6 for control group empty. n=15,5,10 for defect groups in order). *p<0.05 vs. native control tissue.

The local shear modulus of the control cartilage showed variation with depth, with the minimum modulus value occurring within 100μm of the articular surface (Figure 3.5A, B,C).

In contrast, local shear moduli of the repaired cartilage defects were significantly lower than control tissue, showing no minimum or variation with depth. Next we compared the moduli for Gmin (averaged 50-150μm) and $G_{plateau}$ (200-1000μm) values for defect and control groups(Figure 3.5D,E,F). We found Gmin for cartilage defects was 1.5-2 times lower than that for control cartilage; whereas the $G_{plateau}$ values were 7-10 times lower than those of native tissues (Figure 3.5D,E,F).

3.5 DISCUSSION

The goal of the present study was to provide a more thorough characterization of the mechanical performance of repaired cartilage implants than has been reported previously. MACI® implants were tested in a large animal defect model for over 1 year; and revealed overall better defect filling, toluidine blue reactive matrix, and collagen type II staining compared to ACI-Maix™ membranes alone or paired empty defects. Furthermore, a total of 276 samples harvested from implants and controls were tested to measure friction, compressive, and shear properties. These data show a range in implant performance, with frictional properties of all implants similar to control, compressive modulus of MAIX™ and empty implants were different from controls, and shear properties for all groups that differed significantly from controls.

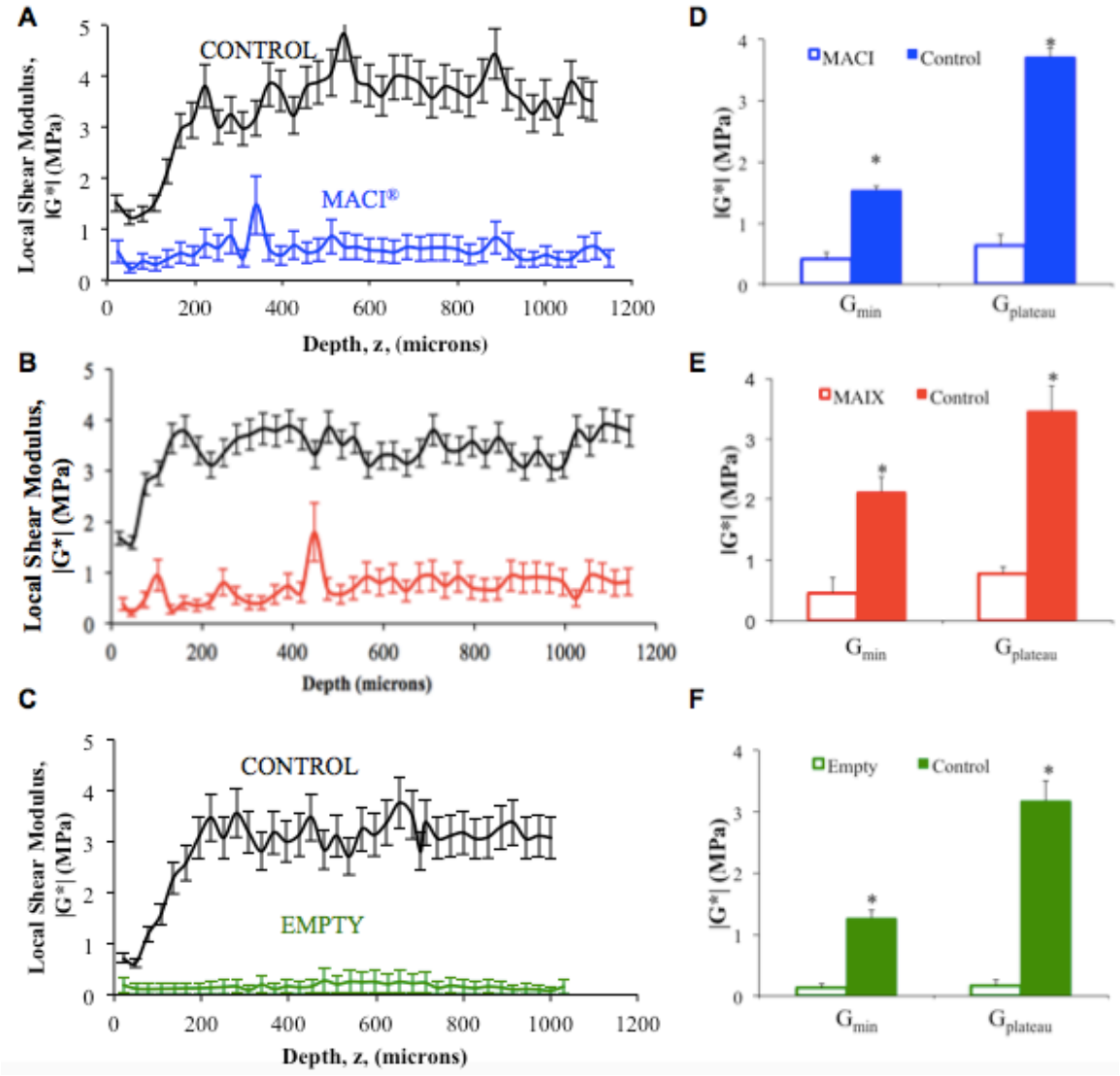

Figure 3.5 (A, B, C) Local shear modulus profiles for tissue samples harvested from each of the implant groups tested. **(D, E, F)** G_{min} (averaged 50-150μm) and $G_{plateau}$ (averaged 200-1000μm) values for defect and control groups. *p<0.001 vs. native control tissue.

Previous research involving the mechanical performance of MACI grafts report average compressive stiffness values ranging from 16-50% of native cartilage. In our confined compression testing, defects filled with MACI® grafts performed relative to their contralateral control (70%). The average aggregate modulus and hydraulic permeability of the MACI® groups were not statistically different from the control tissue (Figure 3.3A, B). The MACI® grafts in this study had an aggregate modulus that was 70% of native cartilage on average. Some of the increased performance of these MACI® grafts may be attributed to the long-term implant duration and the use of a large animal model.

The healthy function of engineered or repaired tissue and its contacting body (i.e. the apposing meniscus or cartilage), may be dependent on providing a low friction surface during articulation [57,64,65]. Consequently, researchers have turned towards different mechanical and chemical stimuli during pre-implantation culture to promote effective lubrication [66, 67, 56]. Previously, *in vitro* studies have shown that although frictional properties of tissue repair scaffolds can be significantly higher than native cartilage, the localization of lubricants on the scaffolds can effectively reduce friction coefficients [56,54,68,69]. Similarly, in a meniscus repair study, scaffolds that were tested before and after *in vivo* implantation exhibited progressively lower friction coefficients as a function of implant time [57, 58]. In this study, the tribological characterization revealed no significant differences between all sample groups and native cartilage. Such data are consistent with the idea that at one year of implantation, these implants are sufficiently capable of localizing boundary lubricants to enable

functional lubrication.

During confocal strain mapping, defects performed significantly worse than their contralateral normal controls, regardless of treatment condition (Figure 3.4B). Local spatial shear profiles revealed the depth dependent modulus for control and repaired tissue(Figure 3.5). Control tissue showed large variation of modulus in depth; while, engineered tissue showed 4-10 times lower modulus in both the minimum and plateau moduli.

The low shear modulus of all the grafts makes any repaired cartilage susceptible to mechanical failure or degradation. Previous studies have shown that shear properties of normal cartilage are highly dependent on collagen content and organization [60,70]. Tissue from repaired cartilage defects is known to have different collagen fiber size and organization compared to normal tissue [59], which is consistent with our current observations that global and local shear properties do not match native tissue. It should be noted that reduction in |G*| probably arises from lack of organized collagen within repaired tissue grafts; this is consistent with predictions of network-based models of cross-linked polymers [71]. These models predict that below critical values of fiber concentration, size, and connectivity, the shear modulus vanishes. Only after the percolation threshold is achieved does shear modulus increase dramatically. Based on the data in the current study, it seems likely that repaired cartilage in all groups is a loose, discontinuous collagen network that is near the rigidity percolation threshold. As such, ensuring sufficient collagen concentration, size, and connectivity may be of particular importance for improving cartilage repair and overall performance of any cartilage repair procedure.

MACI® implants show promise for repairing osteochondral defects and in matching compressive and frictional properties of native cartilage; however, attention should be focused on improving the shear properties of such implants. The results underscore that histologic assessment and biochemical analysis alone are not sufficient for predicting the mechanical performance of cartilage grafts. Histologic analysis indicated that MACI® grafts (Figure 3.2) improved chondrocyte proliferation and GAG content over empty defects, however, biomechanical benefit was only evident in aggregate modulus and hydraulic permeability (Figure 3.3) and not in the shear properties (Figure 3.5). The relationship between structure and function is quite complex in repaired tissue and may differ even from that of native cartilage. As such, thorough mechanical evaluation of such implants is critical to assessing the performance of repaired cartilage.

3.6 ACKNOWLEDGMENTS

The authors gratefully acknowledge Natalie Galley and Jessie Silverberg for their discussions and contributions. Genzyme Corporation, Cornell University, Diversity Programs in Engineering, Cornell Veterinary Medicine, and the National Science Foundation Graduate Research Fellowship supported this work.

CHAPTER 4

MECHANICAL PROPERTIES AND STRUCTURE-FUNCTION RELATIONSHIPS IN ARTICULAR CARTILAGE REPAIRED USING IGF-I GENE-ENHANCED CHONDROCYTES[§]

4.1 ABSTRACT

Several studies have demonstrated the benefits of IGF-I gene therapy in enhancing the histologic and biochemical content of cartilage repaired by chondrocyte transplantation. However, there is little to no data on the mechanical performance of IGF-I augmented cartilage grafts. This study evaluated the compressive properties of full-thickness chondral defects in the equine femuropatellar joint repaired with and without IGF-I gene therapy. Animals were randomly assigned to one of three study cohorts based on chondrocyte treatment provided in each defect: 1.) IGF-I gene delivered by recombinant adeno-associated virus (rAAV)-5; 2) AAV-5 delivering GFP as a reporter; 3) Naïve cells without virus. In each case, the opposite limb was implanted with a fibrin carrier without cells. Samples were prepared for confined compression testing to measure the aggregate modulus and hydraulic permeability. All treatment groups, regardless of cell content or transduction had mechanical properties inferior to native cartilage. Overexpression of IGF-I increased modulus and lowered permeability relative to other treatments. Investigation of structure-property relationships revealed

---

[§]Griffin, D., Ortved, K., Nixon, A., Bonassar, L. "Mechanical properties and structure-function relationships in articular cartilage using IGF-I gene therapy," Journal of Orthopedic Research, in review.

that Ha and k were linearly correlated with GAG content, but logarithmically correlated with collagen content. This provides evidence that IGF-I gene therapy can improve healing of articular cartilage and can greatly increase the mechanical properties of repaired grafts.

4.2 INTRODUCTION

Autologous chondrocyte implantation (ACI) into articular cartilage defects has been used clinically for over twenty years with the goal of preventing further cartilage degeneration and progression of osteoarthritis[72]. The procedure involves harvesting non-weight bearing articular cartilage and enzymatically removing the extracellular matrix to isolate the chondrocytes. Historically chondrocytes were contained in the defect using a periosteal flap[72], while more recently type I/type III collagen membranes have been used in conjunction with fibrin sealants. This technique has shown promising results in equine and human patients with production of hyaline-like repair tissue following transplantation of chondrocytes into chondral defects[73,74]. Despite the potential for hyaline-like tissue, ACI repairs still contain a significant percentage of fibrocartilage. Thus, repair tissue may be further improved through the genetic manipulation of the autologous chondrocytes.

Genetically modified chondrocytes that express insulin-like growth factor-I (IGF-I) have been shown to improve cartilage repair over naïve cells in a variety of animal models, including rabbit, dog, and horse [75,76,77,78,79]. IGF-I transfection increased aggrecan and type II collagen content in cartilage repair, and improved integration with surrounding cartilage matrix[78]. Many studies have shown the benefits

of grafts using autologous chondrocytes, but few have analyzed the mechanical properties of the repaired tissue [78,80,81]. Particularly, there is little to no mechanical data on the restorative effects of IGF-I in ACI grafts in a large animal model.

Notably, recent work has demonstrated that adeno-associated virus (AAV) transduction and transplantation of chondrocytes greatly improves appearance and biochemical composition of repaired cartilage[82]. Particularly rAAV5-IGF-I group resulted in significantly better healing at 8 week arthroscopy and 8 month examination when compared to controls. At 8 months, defects implanted with cells expressing IGF-I had better histological scores compared to control defects and defects repaired with naive chondrocytes. This included increased chondrocyte predominance and collagen type II, both features of hyaline-like repair tissue[83]. rAAV5-IGF-I enhanced collagen type II in defects compared to all other treatment groups. GAG content of repair tissue at 8 months post-implantation was significantly higher in the IGF-I group compared to GFP group. However, there were no significant differences in GAG between chondrocyte IGF-I, naïve chondrocytes, and fibrin-treated defects.

However, the mechanical function of these tissues is unknown. In contrast to the lack of mechanical data on the performance of cartilage grafts many studies report on the biochemical composition of repaired cartilage using histology or biochemical assays. The biochemical composition of repaired cartilage is thought to be a good surrogate for the mechanical properties of the tissue with compressive properties of healthy adult cartilage attributed primarily to the proteoglycan content[84,85,86,87]. However, the relationship between the composition and mechanical properties of repaired cartilage is not well understood. More recently, collagen content has shown to

be important in the properties of younger tissue[88,89,90,91]. With this in mind, the goal of the present study was to evaluate the compressive properties, composition, and structure property relationships of cartilage repaired in full-thickness chondral defects with and without IGF-I gene therapy at 8 months in an equine model.

4.3 MATERIALS AND METHODS

4.3.1 Graft Preparation

As described previously[82], chondrocyte implantation was performed on a total of 24 skeletally mature 2-4 year old horses using a protocol approved by the Institutional Animal Care and Use Committee of Cornell University. Briefly, horses were first anesthetized and articular cartilage (2-3g) was arthroscopically harvested from the distal non-weight bearing portions of the medial and lateral trochlear ridges of one randomly selected talus. Chondrocytes were isolated, expanded in monolayer culture to a total of approximately $20x10^6$ cells, and then transduced 48 hours prior to surgery in Opti-Mem (Invitrogen, Grand Island, NY) rAAV5-IGF-I (n=8), rAAV5-GFP (n=8), or naïve cells with no virus as a negative control (n=8). Cells were transduced for 2 hours with a viral dose of 10^5 viral genomes/cell. Following transduction, chondrocytes were suspended in cryoprecipitated autogenous fibrinogen that was prepared from previously collected plasma[82].

4.3.2 Implantation Surgery

Bilateral full-thickness chondral defects that extended down to, but not through, the subchondral plate, were created on the lateral trochlear ridge of both femurs using a 15mm diameter fluted spade-bit cutter with a sharpened perimeter skirt (Special Devices, Grass Valley, CA) under arthroscopic guidance. Each horse served as its own control with one defect being grafted with chondrocyte/fibrin mixture and the contralateral defect grafted with fibrin alone.

4.3.3 Tissue harvest

At 8 months post-implantation, horses were euthanized and a 3mm x 20mm osteochondral block was harvested from the defect, immersed in protease inhibitors, snap-frozen in liquid nitrogen, and stored at -80°C for mechanical testing. Separate osteochondral blocks and cartilage segments were collected for toluidine blue staining, and type II collagen immunohistochemistry, and biochemical analyses including GAG quantification using the DMMB assay and type II collagen quantification using ELISA (Chondrex, Redmond, WA)[84].

4.3.4 Histology & Immunohistochemistry

As described previously[82], osteochondral blocks were fixed in 4% paraformaldehyde, decalcified in 10% ethylenediamine-tetra-acetic acid (EDTA) (Sigma-Aldrich, St. Louis, MO) prior to embedding in paraffin, and sectioned at 6μm. Osteochondral sections were then stained with toluidine blue to evaluate proteoglycan content. Type II collagen immunohistochemistry was performed following deparaffinization, rehydration, and treatment with hyaluronidase (Sigma-Aldrich, St.

Louis, MO). Sections were then blocked with normal goat serum and incubated with polyclonal rat anti-bovine type II collagen primary antibody (1:100)(courtesy of Dr. Michael Cremer, VA Hospital, Memphis, TN). A secondary biotinylated goat-anti-rat antibody (ABC Staining System, Santa Cruz Biotechnology, Dallas, TX) was applied, followed by streptavidin conjugated peroxidase to catalyze chromagen development in 3,3'-diaminobenzidine tetrachloride (Sigma-Aldrich, St. Louis, MO), and counterstaining with haemotoxylin.

4.3.5 Confined Compression

Methods for analysis of the compressive properties of cartilage were based on those described previously[79]. 48 full thickness cylindrical plugs (3 mm diameter) were harvested from the defect region using a biopsy punch (Miltex, York, PA) applied perpendicular to the articular surface. Remote area (n=5) specimens, away from implanted defect, were obtained as a native control. The plugs were thawed in a bath of PBS containing protease inhibitors (Invitrogen, Carlsbad, CA). Prior to testing, sample heights were measured using a caliper. Samples were placed in a 3 mm confining chamber, covered with a porous plug and PBS with protease inhibitors (Sigma-Aldrich, St. Louis, MO), and mounted to a EnduraTEC ELF 3200 (Bose, Eden Prairie, MN) for testing. A series of 5% steps in compressive strain were imposed on each sample up to a total of 40% strain. For each step, the resultant load was measured for 10 minutes using a Honeywell 50lb load cell (Bose, Eden Prairie, MN) at a frequency of 1 Hz. The stress-relaxation curves were fit to a poroelastic model and analyzed using custom MATLAB code to calculate aggregate modulus (Ha) and

hydraulic permeability (k) [54,55].

4.3.6 Statistics

For equilibrium modulus and hydraulic permeability data a one-way mixed model analysis of variance test was performed between all testing groups to determine the effects of the presence of cells, the transduction by AAV, and the specific effects of IGF-I. Further, this analysis compared repaired tissue to healthy tissue from remote locations. To determine the relationship between composition and mechanical properties, the presence of GAG on Ha and k was determined by linear regression while the effect of collagen content was determined by logarithmic regression. For both tests differences or regressions were considered significant for $p < 0.05$.

4.4 RESULTS

4.4.1 Histology & Immunohistochemistry

Photomicrographs of osteochondral sections taken from repair tissue at 8 months post-implantation showing proteoglycan and type II collagen formation are presented in Figure 4.1. Defects implanted with chondrocytes overexpressing IGF-I had the most toluidine blue staining on histochemical sections compared to the other treatment groups. Similarly, type II collagen immunoreaction revealed more staining in AAV-IGF group compared to other treatment groups.

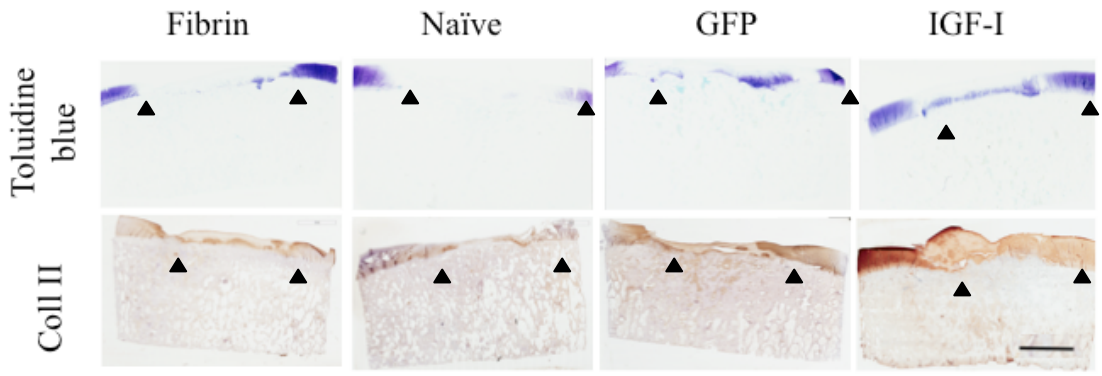

Figure 4.1. Photomicrographs of osteochondral sections taken from repair tissue at 8 months post-implantation and stained with toluidine blue to evaluate proteoglycan content and type II collagen immunohistochemistry (scale bar = 5mm). Black arrows denote defect boundaries.

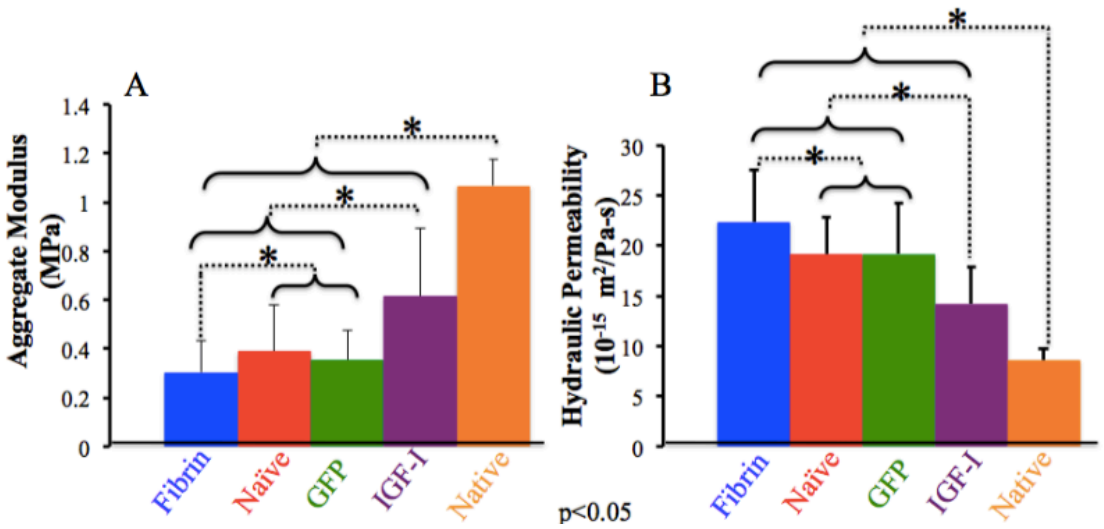

Figure 4.2 (A) Aggregate modulus and **(B)** hydraulic permeability of repaired tissue at 8 months. All data groups are displayed as mean values with standard deviations noted by error bars. Dash lines represent significant differences between groups; Differences were considered significant for $p < 0.05$.

4.4.2 Compressive Properties

The aggregate modulus for native tissue remote to the defect ranged from 1.0-1.2 MPa while hydraulic permeability ranged from 7-8×$10^{-15}$$m^2$/Pa-s both of which are consistent with previous reports on the properties of adult equine cartilage[79,89]. Cartilage repaired using chondrocytes overexpressing IGF-I had an equilibrium modulus that was 60% of remote native cartilage (Figure 4.2A), while rAAV5-GFP, naïve, and fibrin constructs had aggregate moduli that were 37% ($p<0.05$), 41% ($p<0.05$), and 26% ($p<0.05$) of control, respectively. The hydraulic permeability of IGF-I constructs was 1.5 times higher than control tissue, but was significantly lower than other treatment groups, which ranged from 2.5 to 3.5 times higher than native control tissue (Figure 4.2B). Hydraulic permeability of repaired tissue from constructs containing cells (naïve and GFP-labeled) was lower than that of tissue formed from acellular fibrin constructs ($p<0.05$).

4.4.3 Structure-property relationship

To determine the extent to which the properties of the tissue formed depended on composition, data from all repaired and remote cartilage samples were pooled and compared to GAG content as measured by the DMMB assay[82]. For this pool of 53 samples, the aggregate modulus was positively correlated ($R^2=0.53$, $p<0.00001$) with GAG content; while, the hydraulic permeability was weakly negatively correlated ($R^2=0.21$, $p<0.00022$) with GAG content (Figure 4.3). A similar approach was taken

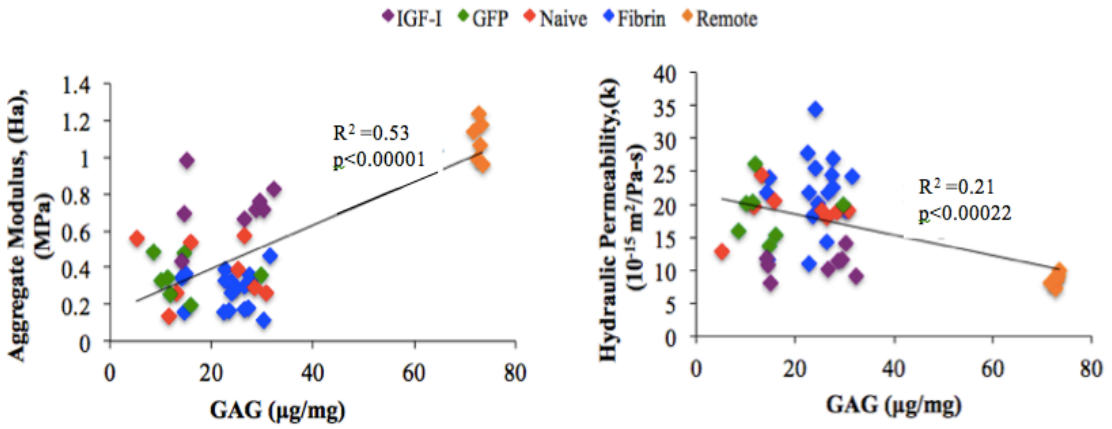

Figure 4.3 Structure-function correlations of native and repaired tissue properties at 8 months. All correlations were found to be statistically significant. GAG/DW demonstrated a linear trend with positive weak correlations in Ha (R^2=0.53) and k (R^2=0.21) for repaired tissue.

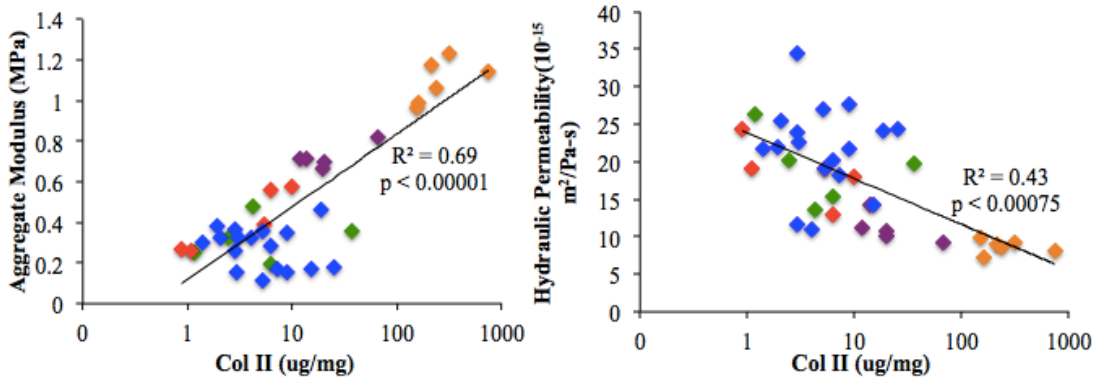

Figure 4.4 Structure-function correlations of native and repaired tissue properties at 8 months. All correlations were found to be statistically significant. Col II/DW demonstrated a linear trend with positive weak correlations in Ha (R^2=0.69) and k (R^2=0.43) for repaired tissue.

determine the effect of collagen content on compressive properties. In this case, the aggregate modulus was logarithmically correlated with collagen content (R^2 =0.69, $p<0.00001$), while hydraulic permeability was negatively logarithmically correlated (R^2 =0.43, $p<0.00075$) with collagen content (Figure 4.4). Notably, these correlation coefficients were higher for collagen content than for GAG content.

4.5 DISCUSSION

This study evaluated the compressive properties and structure-function relationships of full-thickness chondral defects repaired by ACI with and without IGF-I gene therapy in a long-term equine model. The presence of cells enhanced mechanical properties, transduction of the reporter gene, GFP, had no effect, while over expression of IGF-I increased modulus and lowered hydraulic permeability relative to all other treatment groups. Repaired cartilage receiving IGF-I had an aggregate modulus that was 60% of normal cartilage. All treatment groups, regardless of cell content or transduction had mechanical properties inferior to native cartilage.

To date, there is limited data describing the mechanical performance of cartilage grafts in long term large animal models, which is arguably the most important parameter for predicting the clinical success of grafts [86]. Previous mechanical testing on cartilage that was repaired using autologous chondrocytes has reported mixed results. Confined compression testing on ACI repaired tissue showed an aggregate modulus that was only 12% of native tissue at 8 months in an equine model [84,91]. Stiffness tests in an ovine model with matrix-induced autologous

chondrocyte implantation (MACI) grafts with a type II collagen membrane ranged from 37-50% of native cartilage at 12 months[86]. MACI grafts with a type I/type III collagen membrane in an equine model was shown to have an aggregate modulus that was 70% of native tissue at 12 months[79]. IGF-I augmented cartilage grafts in this study had an aggregate modulus that was 60% of native cartilage at 8 months, with non-transfected cellular grafts ~40% of native cartilage.

It is widely believed that compressive properties of cartilage in confined compression depend primarily on GAG content, with collagen playing only a minor role [86,89,90,87,88]. However, it is unclear if such relationships hold for repaired cartilage. In the current study, investigation of structure-property relationships revealed that Ha and k were weakly correlated with GAG content, but logarithmically correlated with collagen content. In all repaired groups, the GAG contributes to compressive properties similarly for all tissue compositions. Correlations between Ha, k, and GAG content were statistically significant but there was significant variation in data for repaired tissue. Notably, IGF-I groups had higher modulus and lower permeability than would be predicted from the linear correlation. In contrast, fibrin alone samples had lower Ha and higher k than would be predicted. More specifically, previous data on the tissues show no significant difference in GAG content[82], which would predict minimal difference in confined compression modulus. To understand whether other components of the matrix were contributing to the compressive modulus, we performed correlation analysis on the role of collagen in contributing to the mechanical behavior.

Indeed, there was a clear relationship between Ha, k, and collagen content;

however, this correlation was logarithmic (Figure 4.4). As a consequence of this logarithmic relationship, there was little variation in Ha and k at high collagen concentrations (i.e. > 50μg/mg). In this range, a 4-fold increase in collagen increased Ha by only 40% and decreased k by < 10%. In contrast, at low collagen content (< 50μg/mg) Ha and k varied greatly with collagen content. For example, increasing collagen content from 10 to 20μg/mg increased Ha 9-fold and decreased k 4-fold. These results suggest that collagen may have a particularly important mechanical role in the compressive properties of repaired cartilage at early stages of maturation.

Although it is well accepted that the GAG content contributes most directly to the compressive properties for adult cartilage [86,90], collagen density has also shown to contribute positively to the compressive modulus in young animals[19]. The compressive properties of cartilage from 1 to 3 week-old bovine calf and from young adult correlated with both GAG and collagen content. Intriguingly, these development-associated changes in biomechanical properties were primarily associated with a marked (2-3-fold) increase in collagen content and no detectable change in GAG content. As such, the evolution of structure-property relationships in repaired cartilage in adults may parallel that in cartilage development in young animals.

Collectively these data suggest that structure-property relationships are different for native and repaired tissue. Although obtaining native properties remains a challenge, this study demonstrates that rAAV5-IGF-I *ex vivo* gene therapy is an effective method to enhance mechanical performance of repaired cartilage. Further investigation into structure-function relationships and genetically-modified chondrocytes show promise for improving hyaline features of repaired cartilage.

4.6 ACKNOWLEDGMENTS

This research supported by Cornell University, Cornell Vet. Medicine, Cornell University Provost Diversity Fellowship, and NIH 5R01-AR055373. In addition, a special thanks to Katherine Hudson and Brandon Borde for their contributions.

CHAPTER 5

DETECTION AND CHARACTERIZATION OF LOCAL INTERFACIAL MECHANICS IN A CARTILAGE DEFECT REPAIR MODEL[#]

5.1 ABSTRACT

The lack of lateral anchoraging and integration of grafted cartilage makes the tissue more susceptible to mechanical failure. Recently, our lab has developed a novel system for measuring the microscale mechanics of native and repaired tissue on the length scale of 20μm. This approach would provide new information about the mechanical environment at the interface of repaired and host native cartilage. The objective of this study was to detect and characterize the local mechanics at the interface of repaired and native articular cartilage. Either fresh cells or cell clusters formed over 14 days were placed in a cartilage ring with a 6mm inner diameter, implanted subcutaneously in female nude mice and harvested at 12 weeks. Samples of the interface were cut into ~2mm cubes (Fig. 2B) and prepared for confocal strain mapping (Fig. 2C, D). Localized strains were measured using particle image velocimetry (PIV) as described previously. Shear deformation was induced by displacing the moveable plate in the direction parallel to the articular surface to produce 1% shear strain. Vector maps and plots of γ_{xy} and ε_{yy} exhibited large strains at the interface. γ_{xy} were lower near the articular surface, and higher in the deep zone. ε_{yy} were higher near the articular surface and remained consistently high in the deep

[#]Griffin, D., Meppelink, A.(MGH), Randolph, M.(MGH), Bonassar, L. "Detection and characterization of local interfacial mechanics in a cartilage defect repair model," in preparation

zone(Fig. 3). Additionally, there was a high degree of peeling along the interface, which could infer a new probable delaminating mechanism (Fig. 4). These results shed more light on the mechanical properties for strategic engineered constructs to withstand physiological loads and promote integration in cartilage repair.

5.2 INTRODUCTION

Currently, a number of techniques are used for articular cartilage repair, such as subchondral penetration[91,92,93], osteochondral transplantation[94,95,96], autologous chondrocyte transplantation[97,98,99], as well as tissue-engineered grafts[100,101,102]. A major challenge in achieving successful cartilage repair is the integration of repaired cartilage with the adjacent native cartilage. The lack of lateral anchorage and integration of repair or graft tissue leaves the graft susceptible to mechanical failure that could lead to poor prognosis[103,104,105,106,107]. This problem has motivated a great deal of research into methods of enhancing the integration of repair tissue with the surrounding host cartilage.

In vivo studies normally evaluate cartilage repair with biochemical assays and histological methods [95,118,110]; however, the biomechanical behavior of this interface is poorly understood. There have been many studies that measured strength of the integration of cartilage-graft interfaces, including *in vitro* model, subcutaneous or heterotopic *in vivo* models, and orthotropic transplants into joint defects. Such studies have measured integration strength with lap-shear tests[98,103], tensile tests[109] and push out model tests[107,106]. Only a handful of studies have characterized the compressive properties of repair tissue through confined compression[110] indentation[113] and one

paper reporting integration strength and tensile properties of repaired tissue from an *in vivo* joint defect[115]. Generally these studies have investigated bulk tissue properties; such as failure strength, stiffness, and failure strain[111,113,115].

This lack of data is in part due to the fact that previous techniques are unable to measure local deformations at such interfaces. As such there is essentially no information on the local deformations that occur at these interfaces during failure. Measuring the deformations would help to identify local mechanisms of tissue failure as well as locate regions of this interface that may be particularly susceptible to failure. Such knowledge would provide a valuable tool for assessing the efficacy of cell-based cartilage repair methods and then inform techniques to improve functional cartilage graft integration.

Our group has developed a novel system for measuring the local mechanics of native and repaired cartilage via confocal elastography[92,100,120,91,95]. Specifically this technique has measured local shear properties of cartilage on length scale of 20-40μm[122,123,124,125], and has identified large regional variations in mechanical properties along the depth of the tissue. However to date these techniques have not been applied to understanding local mechanics of cartilage-graft interfaces. Therefore the objectives of this study were to: 1) characterize the local mechanics at the interface of repaired and native articular cartilage in a subcutaneous heterotopic transplant model; and 2) assess the effect of chondrocyte culture conditions on the mechanical behavior of the interface.

5.3 METHODS

5.3.1 Tissue Preparation/ Implantation

Integration of the engineered tissue with existing native cartilage was examined in a system in which engineered cartilage was grown in a cylindrical defect punched in an articular cartilage explant (Fig. 1A, B). The Institutional Animal Care and Use Committee of the Massachusetts General Hospital following the National Institutes of Health Guide for the Care and Use of Laboratory Animals approved all procedures involving animals. Articular cartilage was aseptically harvested from the knees of Yorkshire pigs. Articular cartilage was dissected sharply from the underlying bone and minced into 1- to 2-mm fragments under sterile conditions. The cartilage was then digested with 0.1 w/v% collagenase type II (Worthingon, Freehold, NJ) for 12 to 18 hours at 37°C. After digestion, chondrocytes were rinsed and washed twice with chondrocyte growth media. Cell number was determined using the trypan blue dye test. After isolation, the chondrocytes were combined with fibrin gel by two different methods. In the first group, $10x10^6$ cells were placed into a 15 cc polypropylene tube and cultured statically at 37°C for 14 days; producing cell clusters. Chondrocyte growth media containing Ham's F-12 media (Invitrogen, Carlsbad, CA) supplemented with 10% fetal bovine serum (Invitrogen), 1% non-essential amino acids (Invitrogen), 1% antibiotic antimycotic solution (Sigma, St. Louis, MO) and 0.005% ascorbic acid (Sigma) was used for cell culture and changed every 3 to 4 days. Cell clusters were placed in the center of a devitalized 6mm inner diameter swine articular cartilage ring and capped with fibrin gel (Sigma)[112] (Fig. 1B). In the control group, fresh chondrocytes containing no pre-culture were immediately encapsulated in

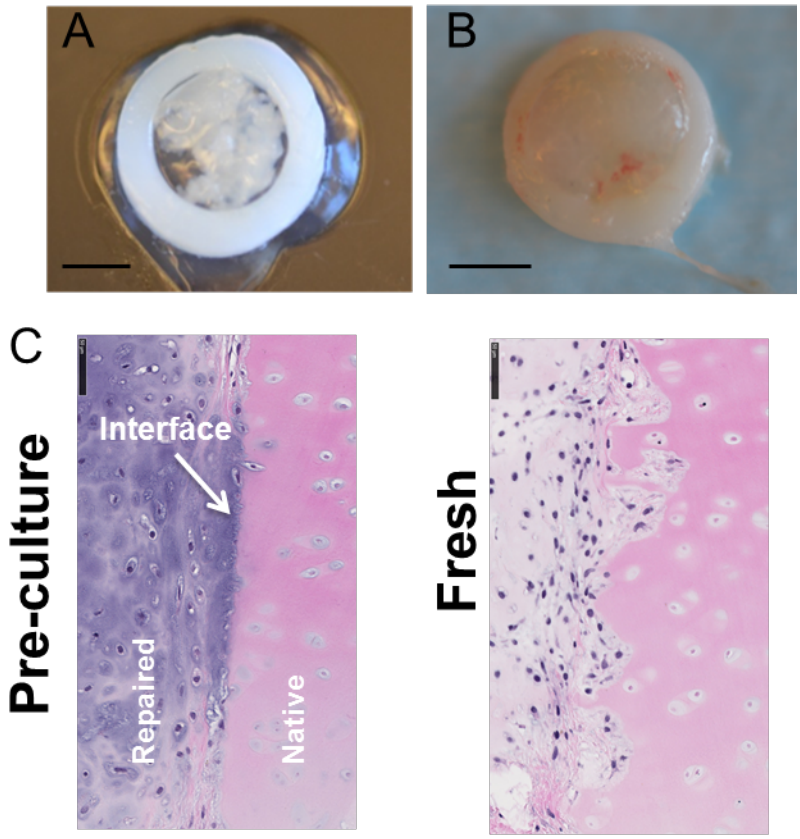

Figure 5.1. Cell clusters capped with fibrin gel in the center of cartilage ring prior to implantation (A) and after harvest after 12 weeks in vivo (B). Scale bars = 300μm. H&E stain, showing interface of repaired and native articular cartilage in the murine model (C) Scale bar = 1mm.

fibrin gel as a cell suspension of 40 million cells per mL and injected into the center of devitalized swine articular cartilage ring.

To assess the maturation of the interface between new cartilage and native cartilage, constructs generated as described above were implanted subcutaneously in nude female mice. As described previously, although not a load-bearing model subcutaneous implantation enables rapid construct development under *in vivo* conditions[126,127]. Filled cartilage rings were implanted subcutaneously in the dorsum of nude female mice (*nu/nu* mice; Massachusetts General Hospital, Boston, MA) and harvested at 12 weeks (n=5). The center of the cartilage disk was removed using a 3mm biopsy punch leaving a ring of engineered and native matrix (Fig. 2A). The rings were sliced into 2mm cubes and prepared for mechanical testing to observe local deformations under shear (Fig. 2B).

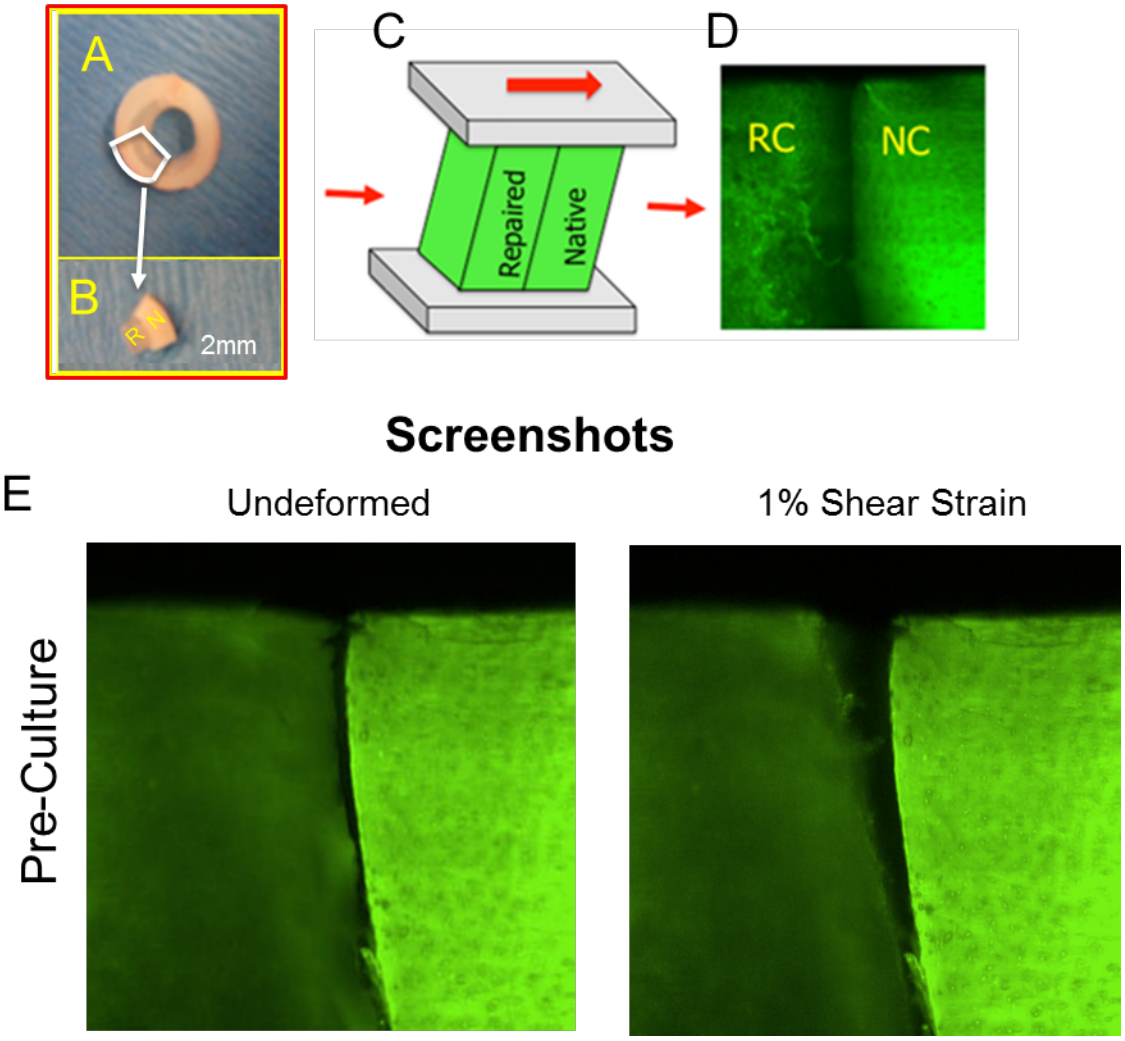

Figure 5.2. Articular rings of repaired and native cartilage were cut into cubes (A, B) representative schematic of how the sample is loaded in the tissue deformation imaging stage (C) confocal micrograph taken at the interface of repaired cartilage (RC) and native cartilage (NC) (D) screenshots of underformed and deformed at 1% shear strain.

5.3.2 Histology

Constructs from each group were randomly selected and fixed in 10% phosphate-buffered formalin for 48 hours. Samples were embedded in paraffin and 5μm sections were cut from the middle of the constructs. Sections were stained with hematoxylin and eosin (H&E) to assess morphology of the engineered constructs and integration of the constructs with the cartilage ring. Briefly, sections were stained with hematoxylin (Leica, Buffalo Grove, IL) for 10 minutes, followed by brief exposure to 0.25% acid alcohol and vintage bluing reagent (StatLab, McKinney, TX), and finally stained with eosin (Leica) for 90 seconds.

5.3.3 Confocal Elastography

2mm cubes were placed into a 7 μg/mL of 5-isomer of fluorescein dichlorotriazine (5-DTAF) (Molecular Probes®, Grand Island, NY) solution for 30 min to fluorescently stain the cartilage extracellular matrix[120,121,122,123,124]. The deep zone of the cubes were glued to a tissue deformation imaging stage (TDIS) and compressed to 7% axial strain (Fig. 2C). The TDIS was mounted on an inverted Zeiss Live 5 confocal microscope and imaged using a 488 nm laser (Fig. 2D). Sinusoidal shear deformations were induced by displacing the moveable plate in the direction parallel to the articular surface by 20μm, yielding an effective shear strain of 1% shear strain, and frequency of 1 Hz. Localized strains were measured using a particle image velocimetry (PIV) algorithm implemented in MATLAB[120]. After each increment of shear strain, multiple snapshots 512×512μm were taken throughout the sample and tiled in order to obtain an image spanning the entire tissue. Images were divided into a

grid with 50×50 μm spacing. Using this grid, the displacement fields in the vertical (u) and horizontal (v) directions were calculated by performing particle image velocimetry analysis on confocal images before and after application of shear. These displacement fields used to calculate shear strain γ_{xy} (du/dy)(Fig. 3A) and axial strain ε_{yy} (dv/dy)(Fig. 4A) throughout the sample. To assess spatial variation in local mechanics between samples (n=4), γ_{xy} and ε_{yy} were averaged across y at x= 75μm, 300μm, and 900μm.

5.3.4 Data Analysis

Localized strains were measured using a particle image velocimetry (PIV) graphical user interface[120]. After each increment of shear strain, multiple snapshots were taken throughout the sample and pieced together in order to obtain an image spanning the entire tissue. The horizontal and vertical displacement field of cells in 512×512 μm[122] windows was calculated by performing particle image velocimetry analysis on confocal images before and after application of shear. Cell positions and displacements were obtained via PIV, and used to calculate shear strain γ_{xy} (du/dy) and axial strain ε_{yy} (dv/dy) at the interface.

5.4 RESULTS

5.4.1 Histology

The H&E staining (Fig. 1) confirmed the formation of new cartilage in both chondrocyte groups, but matrix staining in repaired cartilage was different from that of native cartilage. Constructs created using fresh chondrocytes showed dense cellular

Sliding (γ_{xy})

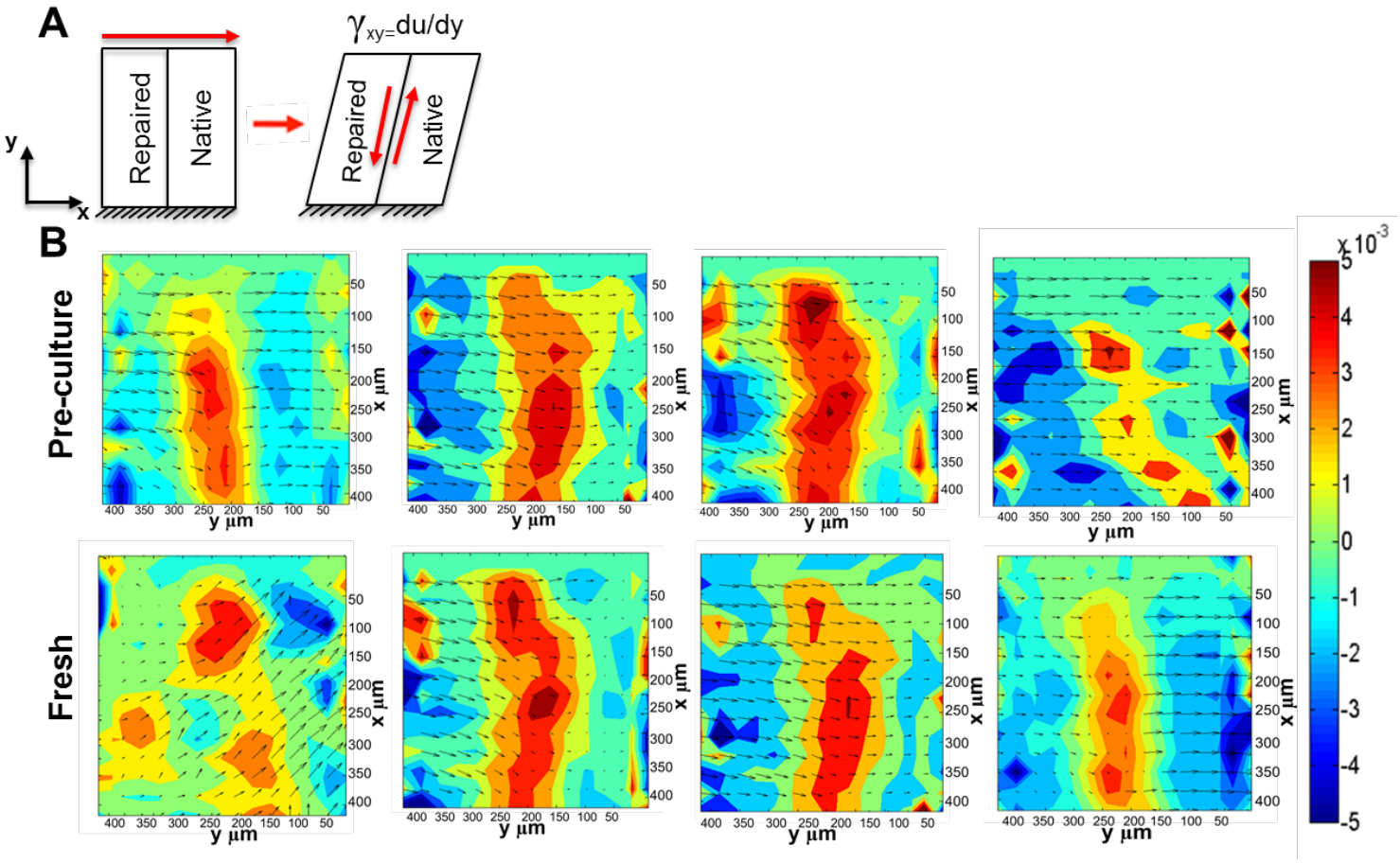

Figure 5.3 Representative schematics of sliding at the interface (A) PIV Vector Maps for Sliding (B) Shear strain applied parallel to the articular surface direction, was found to induce sliding (γ_{xy}) at the interface. Two-dimensional vector maps of γ_{xy} exhibited large strains at the interface for both groups.

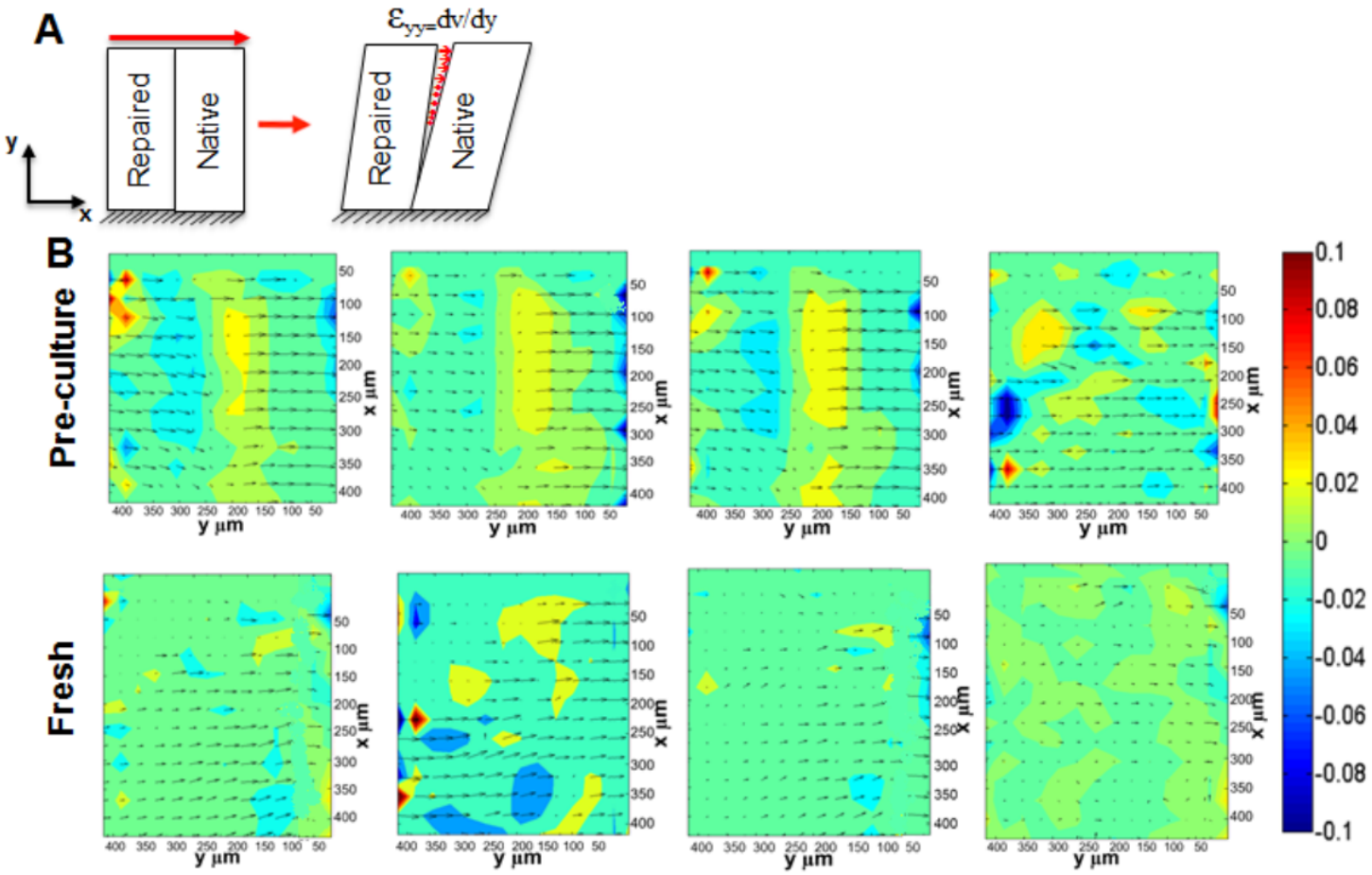

Figure 5.4 Representative schematics of sliding at the interface (A) PIV Vector Maps for Peeling (B) Shear strain applied parallel to the articular surface direction, was found to induce peeling (ε_{yy}) at the interface. Pre-culture group displayed more peeling at interface compared to fresh group. Integration appeared more prevalent near the surface, but was poorly integrated at deeper depths.

tissue (Fig. 1C), created a close interface between the repaired and native cartilage. Specifically, outgrowths of new cartilage matrix were observed penetrating or migrating into the native cartilage matrix disc. In contrast, the pre-culture group showed some apparent integration, but not as marked as that observed when the fresh chondrocytes were used (Fig. 1C).

5.4.2 Confocal Elastography

Local deformations of the interface between native and engineered tissue were easily visualized using confocal microscopy (Fig. 2E). Based on images of the undeformed and deformed states, local deformation tensors were obtained using particle image velocimetry and differentiated to calculate strain tensors. Specifically, shear strain applied parallel to the articular surface resulted 2 modes of deformation at the interface: 1) sliding, as quantified by γ_{xy} (du/dy) (Fig. 3) and 2) peeling, as quantified as ε_{yy} (dv/dy) (Fig. 4) at the interface. Intriguingly, sliding (γ_{xy}) did occur at interface despite the applied orthogonal 1% shear strain. Furthermore, sliding was confined to ~100μm near the interface with a peak strain of ~0.5%, nearly half of the applied orthogonal shear strain. Qualitatively, both fresh and pre-culture γ_{xy} vector maps were similar; however averaged peak strains were lower the for fresh group (.002) than pre-culture group (.003) ($p<.05$). In both culture groups sliding was more pronounced deeper in the tissue γ_{xy} ~.002-.003) compared to the tissue surface ($p<.0001$), where γ_{xy} ~.001 (Fig. 5).

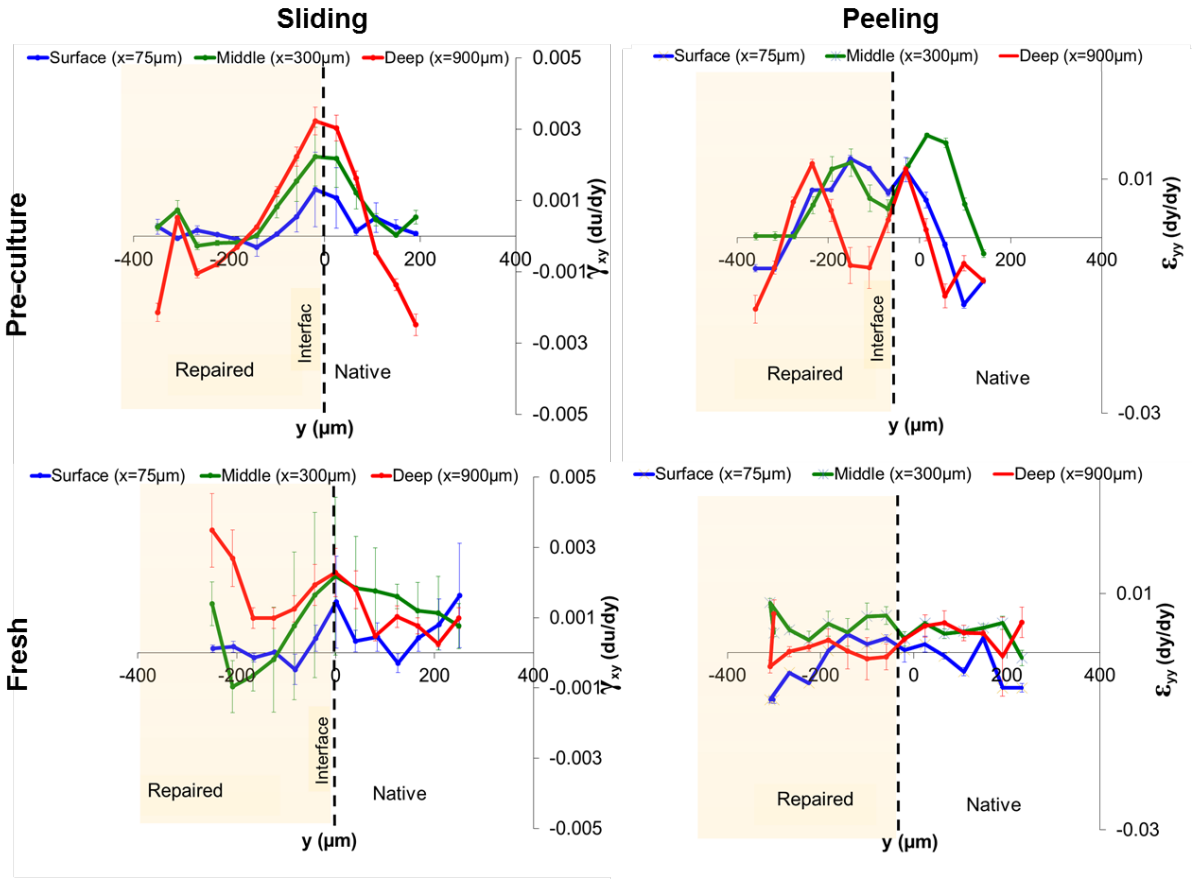

Figure 5.5. Depth-Dependent Interfacial Profiles: The interface in both groups demonstrated very similar sliding features, but was different in peeling. γ_{xy} values were lower at the articular surface, but increased by a factor of 2 at higher depths (300-900μm). ε_{yy} values were higher at the surface and remained relatively high throughout the entire depth of tissue. Bar denotes statistical difference.

Shear loading also induced peeling ε_{yy} (dv/dy) at the interface. Peeling was localized to within ~50μm of interface with a peak strain of ~1.8-2% which was greater than applied shear strain (Fig 4B). The pre-culture group displayed more peeling at interface compared to fresh group (Fig. 4B) ($p<.05$) peak values for pre-culture were >1% at interface and <.25% at interface for the fresh group. Deeper regions of the interface displayed less peeling than the articular surface (Fig. 5) ($p<.05$).

5.5 DISCUSSION

Understanding the mechanical properties at the interface of tissue-engineered cartilage is important for improving integrative repair. The goals of the present study were to characterize the local mechanics at the interface of repaired and native cartilage and to determine if different culture conditions affect the mechanical environment at the interface. The results from this study reveal that shear loading induces a complex, spatially heterogeneous response at the interface between repaired and native cartilage. There were two distinct modes of failure identified at the interface: the sliding along the repaired/native cartilage interface and peeling along the direction of shear. In both fresh and pre-culture groups, there was significant sliding along the interface (Fig. 3). The high compliance of this region suggests a lack of anchorage of engineered tissue to the native tissue. Even though histology indicated a well-bonded interface in the fresh group (Fig. 1C), γ_{xy} values at the interface were as high as .005 (Fig. 3). Additionally, there was minimal peeling in fresh samples, but a high degree of peeling for the pre-culture group (Fig. 4). These data indicate that

chondrocyte culture conditions can affect the quality of integration and mode of mechanical failure.

Many studies routinely evaluate the quality of repair tissue with qualitative or quantitative assays of tissue structure such as gross observations, histology, and immunohistochemistry[128–130]. Such studies have rated integration using histological scoring systems based on continuity of tissue interfaces generated *in vitro* as well as in heterotopic (subcutaneous) or orthotopic *in vivo* transplantation models[115,128,130–133]. Such studies have revealed the importance of matrix synthesis and cell migration in generating continuous interfaces. However, relatively few studies have focused on mechanical evaluation of these interfaces in subcutaneous implantation models. For example, previous studies report time dependent increase in tensile strength, failure strain, failure energy, and tensile modulus to values 5–30% of normal articular cartilage[119,127,128]. Further studies by Gratz et al.[133] and Fujie et al.[134], have reported integration mechanical properties from orthotopic *in vivo* cartilage repair models. In an equine model, Gratz et al.[133] reported the bulk tensile properties of the interface indicating that modulus and strength were 12% and 40% of native tissue respectively. A recently published study by Fujie et al.[134] investigated zone-specific integration properties of repaired articular cartilage defects treated in a porcine model. The authors reported an average tensile strengths of the integration boundary compared to normal cartilage were 12%, 25%, and 45% at the superficial, middle, and deep layers, respectively. Although it was possible to determine the depth-dependent strength of the interface by cartilage zone, this technique involves cutting a full-thickness specimen into three pieces and testing each piece individually. A unique feature of the

present study is that no sectioning was required and this technique allows spatially continuous assessment of 2D strain fields throughout the depth of cartilage. Because our measurement resolution was 20μm, we were able detect mechanical signatures that may have been obscured at the bulk level. Specifically, we were able to identify two mechanisms of failure based on how the tissue deforms at the interface.

Histological assessments are useful in the analysis of integration, but our results suggest that just the appearance of the interface alone may not be enough to predict effective integration. More importantly, the extracellular matrix constituents may play an important role in the mechanical behavior of repairing the interface. For example, previous studies have suggested that collagen[14] and proteoglycans[17] were important for mechanical integration, but these studies used bulk biochemical and mechanical assessments. Thus exploring of structure-function relationship across the interface of engineered and native cartilage might be critical for optimum integration. Previously, we have reported combining confocal elastography, with Fourier-transform infrared imaging (FTIR) to identify key structure-property relationships in the local shear behavior of articular cartilage[121]. Applying this approach of measuring both local composition and mechanics may reveal key factors necessary for robust integration of cartilage implants.

Limitations of this study include an evaluation of cartilage integration in murine subcutaneous model. These models are not optimal as the subcutaneous environment is different from the load bearing native cartilage environment. However, the subcutaneous model have been extensively characterized in helping bridge the gap between *in vitro* and *in vivo* load bearing models in larger animals[119,126,127,135].

Additionally, we do note the sample number was n=4. However, even at low numbers we still identified differences in spatial patterns and culture technique.

In conclusion, this study successfully detected the local interfacial mechanics in a subcutaneous defect repair model. The mechanical characterization of the interface of engineered and native tissue provides us with a powerful tool for studying cartilage integration. These results shed more light on the necessary mechanical properties for strategic engineered constructs to withstand physiological loads and promote integration in cartilage repair.

ACKNOWLEDGMENTS

This study was supported by a Cornell University, Meing School of Biomedical Engineering, the Department of Defense (award number W81XWH-10-1-0791). The authors would like to thank Lena Bartell for her experimental support.

CHAPTER 6

CONCLUSIONS

The experiments described in this thesis research focuses on applying new techniques to understanding how micro-scale mechanical properties of articular cartilage change during tissue degeneration and repair.

We have developed new models for cartilage degeneration in vitro and demonstrated the ability to detect very early signs of tissue damage, which are manifest in mechanical signatures on the length scale of 20 microns. Alterations in local superficial matrix composition, could reveal signatures of early onset osteoarthritis that are not currently available with traditional imaging techniques, presenting new opportunities and new perspectives on cartilage therapies and repair.

In chapters 3 and 4, we have executed measurements of the mechanical performance of cartilage repaired using new biomaterials and gene therapy that have never been made previously. From these data, it is apparent the relationship between structure and function is quite complex in repaired tissue and may differ even from that of native cartilage. Collagen plays an important role in determining the compressive properties of repaired cartilage, particularly at early stages of maturation. Furthermore, the MACI implant (Type I/Type III collagen membrane) does show promise for repairing defects and in matching compressive and frictional properties of native cartilage; though, more attention should be focused on improving the shear properties of such implants. Information obtained from these experiments can help guide the research community with corrective procedures in restoring tissue function

and provide a template for a successful implant design.

Finally, chapter five captures novel mechanical signatures of the interface of native and repaired cartilage that have never been made previously. Via confocal elastography we've demonstrated two distinct error modes for this interface – sliding and peeling. Furthermore, our findings lead to a better interpretation of the mechanical behavior of articular cartilage integration in vivo.

6.2 FUTURE WORK

From this body of work, we've learned poor integration is a common complication with current clinical treatments for focal cartilage repair. More importantly, the extracellular matrix constituents may play an important role in the mechanical behavior of repairing the interface.

Cross-linking collagen has shown to stabilize and strengthen collagen fibers and increase the stiffness of the collagen network. One potential crosslinking agent that has received interest is genipin, a natural plant extract. Genipin cross-linking has been shown to affect the mechanical properties of biological tissues, and type I collagen gels. Genipin cross-linking works by forming intra- and intermolecular crosslinks of the amino residues on tropocollagen. The modified or polymerized form of genipin can stiffen the ECM, adding brides across adjacent collagen fibers. Particularly, the effect of genipin cross-linking on the interface is poorly understood. As such, further investigation of collagen crosslinking with genipin as a technique to improve integration of repaired and native cartilage and to be evaluated as a therapeutic strategy in improving interfacial mechanics.

Chapter 4 provided evidence that IGF-I gene therapy can improve healing of articular cartilage and can greatly increase the mechanical properties of repaired grafts. In terms of the interface, the effect of IGF-I supplementation on interfacial mechanics is poorly understood. Applying this technique may reveal new findings of the restorative effects of IGF on the mechanical behavior of the interface. Clearly, progress exploring such studies requires more detailed experiments coupled with higher-resolution confocal elastography studies that further investigate the mechanical behavior of treatments for focal cartilage repair.

BIBLIOGRAPHY

1. Poole, Robin A et al., "Cartilage Biology: Composition and Structure of Articular cartilage: A template for Tissue repair." Clinical ortho and Related Research. 391S (2001): S26-S33.

2. Buckwalter K.A. An instructional course lecture. Journal of Bone and Joint surgery. 79(1997):612-632.

3. Robi K et al., "The Physiology of Sports Injuries and Repair Processes" Sports and Exercise Medicine" (2000) DOI: 10.5772/54234.

4. Kerin A., Patwari P., Kuettner K, Cole A., Grodzinsky A. (2002) Molecular basis of osteoarthritis: Biomechanical aspects. Cell Mol Life Sci 59: 27–35.

5. W.A Hodge, et al. Contact pressures from an instrumented hip endoprosthesis. J. Bone Joint Surg. [Am], 71 (1989), pp. 1378–1386.

6. Care A. 2002. Pathophysiology and First-Line Treatment of Osteoarthritis, 36:679–686.

7. Lawrence RC, Felson DT, Helmick CG, et al. 2008. Estimates of the prevalence of arthritis and other rheumatic conditions in the United States. Part II. Arthritis Rheum. 58(1):26–35.

8. Ringe J et al., "Regenerative medicine in rheumatic disease—progress in tissue engineering", Nature Reviews Rheumatology 8, 493-498 (August 2012) doi:10.1038/nrrheum.2012.98

9. Carticel. "About Carticel." 2003-2006. Genzyme Biosurgery. March 24, 2006.

10. Ortved KF, Begum L, Mohammed HO, Nixon AJ. 2015. Implantation of rAAV5-IGF-I transduced autologous chondrocytes improves cartilage repair in full-thickness defects in the equine model. [Internet].Mol. Ther. 23(2):363–73.

11. Goodrich LR, Hidaka C, Robbins PD, et al. 2007. Genetic modification of chondrocytes with insulin-like growth factor-1 enhances cartilage healing in an equine model. [Internet].J. Bone Joint Surg. Br. 89(5):672–85

12. Griffin D, Bonnevie E, Lachowsky D, et al. 2015. Mechanical Characterization of Matrix-Induced Autologous Chondrocyte Implantation (MACI®) Grafts in an Equine Model at 53 weeks [Internet].J. Biomech.

13. Care A. 2002. Pathophysiology and First-Line Treatment of Osteoarthritis, 36:679–686.

14. Lawrence RC, Felson DT, Helmick CG, et al. 2008. Estimates of the prevalence of arthritis and other rheumatic conditions in the United States. Part II. Arthritis Rheum. 58(1):26–35.

15. Case JP, Sano H, Lafyatis R, et al. 1989. Transin / Stromelysin Expression in the Synovium of Rats with Experimental Erosive Arthritis.(37):1731–1740.

16. Nguyen Q, Murphy G, Roughley PJ, Mort JS. 1989. Degradation of proteoglycan aggregate by a cartilage metalloproteinase. Evidence for the involvement of stromelysin in the generation of link protein heterogeneity in situ. Biochem. J. 259(1):61–67.

17. Pelletier JP, Martel-Pelletier J, Malemud CJ. 1988. Canine osteoarthritis: effects of endogenous neutral metalloproteoglycanases on articular cartilage proteoglycans. J. Orthop. Res. 6(3):379–388.

18. Chin JR, Murphy G, Werb Z. 1985. Stromelysin, a connective tissue-degrading metalloendopeptidase secreted by stimulated rabbit synovial fibroblasts in parallel with collagenase. Biosynthesis, isolation, characterization, and substrates. J. Biol. Chem. 260(22):12367–12376.

19. Macnauls KL, Hutchinsonsli NI, Toccis J. 1990. Tocci and N I Hutchinson Discoordinate Expression of Stromelysin , Collagenase , and Tissue Inhibitor of Metalloproteinases- 1 in Rheumatoid Human Synovial Fibroblasts.

20. Williamson AK, Chen AC, Masuda K, et al. 2003. Tensile mechanical properties of bovine articular cartilage: variations with growth and relationships to collagen network components. J. Orthop. Res. 21(5):872–880.

21. Elliott DM, Narmoneva D a, Setton L a. 2002. Direct measurement of the Poisson's ratio of human patella cartilage in tension. J. Biomech. Eng. 124(2):223–228.

22. Wilson W, van Donkelaar CC, van Rietbergen B, et al. 2004. Stresses in the local collagen network of articular cartilage: a poroviscoelastic fibril-reinforced finite element study. J. Biomech. 37(3):357–366.

23. Bodine J. et.al, 1978. Flow-independent of articular properties cartilage matrix. J. Biomech. 11:407–411.

24. Zhu W, Mow VC, Koob TJ, Eyre DR. 1993. Viscoelastic shear properties of articular cartilage and the effects of glycosidase treatments.J. Orthop. Res. 11(6):771–781.

25. Buckley MR, Bonassar LJ, Cohen I. 2012. Localization of Viscous Behavior and Shear Energy Dissipation in Articular Cartilage Under Dynamic Shear Loading J. Biomech. Eng. 135(3):31002.

26. Silverberg JL, Dillavou S, Bonassar L, Cohen I. 2013. Anatomic variation of depth-dependent mechanical properties in neonatal bovine articular cartilage. J. Orthop. Res. 31(5):686–91.

27. Oegema TR, Lewis JL, Thompson RC. 1993. Role of acute trauma in development of osteoarthritis.Agents Actions 40(3-4):220–223.

28. Michalek AJ, Buckley MR, Bonassar LJ, et al. 2009. Measurement of local strains in intervertebral disc anulus fibrosus tissue under dynamic shear: contributions of matrix fiber orientation and elastin content. J. Biomech. 42(14):2279–2285.

29. Brightman a O, Rajwa BP, Sturgis JE, et al. 2000. Time-lapse confocal reflection microscopy of collagen fibrillogenesis and extracellular matrix assembly in vitro.Biopolymers 54(3):222–234.

30. Buckley MR, Gleghorn JP, Bonassar LJ, Cohen I. 2008. Mapping the depth dependence of shear properties in articular cartilage. J. Biomech. 41(11):2430–2437.

31. Buckley MR, Bergou AJ, Fouchard J, et al. 2010. High-resolution spatial mapping of shear properties in cartilage. J. Biomech. 43(4):796–800.

32. Pickvance E a, Oegema TR, Thompson RC. 1993. Immunolocalization of selected cytokines and proteases in canine articular cartilage after transarticular loading. J. Orthop. Res. 11(3):313–323.

33. June RK, Fyhrie DP. 2009. Enzymatic digestion of articular cartilage results in viscoelasticity changes that are consistent with polymer dynamics mechanisms. Biomed. Eng. Online 8:32.

34. Rieppo J, Töyräs J, Nieminen MT, et al. 2003. Structure-Function Relationships in Enzymatically Modified Articular Cartilage. Cells Tissues Organs 175(3):121–132.

35. Atkinson TS, Haut RC, Altiero NJ. 1998. Impact-induced fissuring of articular cartilage: an investigation of failure criteria.J. Biomech. Eng. 120(2):181–187.

36. Zernia G, Huster D. 2006. Collagen dynamics in articular cartilage under osmotic pressure.NMR Biomed. 19(8):1010–1019.

37. Head, D. A., A. J. Levine, and F. C. MacKintosh, 2003. Distinct regimes of elastic response and deformation modes of cross-linked cytoskeletal and semi exible polymer networks. Phys. Rev. E 68:061907{1{14.

38. Wilhelm, J., and E. Frey, 2003. Elasticity of polymer networks. Phys. Rev. Lett. 68:061907.

39. Broedersz, C. P., X. Mao, T. C. Lubensky, and F. C. MacKintosh, 2011. Criticality and isostaticity in _bre networks. Nature Phys. 7:983{988.

40. Silverberg, J. et al 2014. Mechanical structure-function relations and rigidity percolation in shear properties of articular cartilage. Biophysical Journal. doi: 10.1529/biophysij.106.089789. Submitted.

41. Inerot S, Heinegård D, Audell L, Olsson SE. 1978. Articular-cartilage proteoglycans in aging and osteoarthritis. [Internet].Biochem. J. 169(1):143–56[cited 2015 Feb 5] Available from: http://www.pubmedcentral.nih.gov/articlerender.fcgi?artid=1184203&tool=pmcentrez&rendertype=abstract.

42. Brittberg M. 2010. Cell carriers as the next generation of cell therapy for cartilage repair: a review of the matrix-induced autologous chondrocyte implantation procedure. [Internet].Am. J. Sports Med. 38(6):1259–71[cited 2015 Feb 5] Available from: http://www.ncbi.nlm.nih.gov/pubmed/19966108.

43. Frenkel SR, Toolan B, Menche D, et al. 1997. Chondrocyte transplantation using a collagen bilayer matrix for cartilage repair. [Internet].J. Bone Joint Surg. Br. 79(5):831–6[cited 2015 Feb 5] Available from: http://www.ncbi.nlm.nih.gov/pubmed/9331046.

44. Willers C, Chen J, Wood D, et al. Autologous chondrocyte implantation with collagen bioscaffold for the treatment of osteochondral defects in rabbits. [Internet].Tissue Eng. 11(7-8):1065–76[cited 2015 Feb 5] Available from: http://www.ncbi.nlm.nih.gov/pubmed/16144442.

45. Peterson L, Brittberg M, Kiviranta I, et al. Autologous chondrocyte transplantation. Biomechanics and long-term durability. [Internet].Am. J. Sports Med. 30(1):2–12[cited 2015 Feb 5] Available from: http://www.ncbi.nlm.nih.gov/pubmed/11798989.

46. Henderson I, Lavigne P, Valenzuela H, Oakes B. 2007. Autologous chondrocyte implantation: superior biologic properties of hyaline cartilage repairs. [Internet].Clin. Orthop. Relat. Res. 455:253–61[cited 2015 Feb 5] Available from: http://www.ncbi.nlm.nih.gov/pubmed/16980901.

47. Laasanen MS, Töyräs J, Vasara AI, et al. 2003. Mechano-acoustic diagnosis of cartilage degeneration and repair. [Internet].J. Bone Joint Surg. Am. 85-A Suppl:78–84[cited 2015 Feb 5] Available from: http://www.ncbi.nlm.nih.gov/pubmed/12721348.

48. Strauss EJ, Goodrich LR, Chen C-T, et al. 2005. Biochemical and biomechanical properties of lesion and adjacent articular cartilage after chondral defect repair in an equine model. [Internet].Am. J. Sports Med. 33(11):1647–53[cited 2015 Feb 5] Available from: http://www.ncbi.nlm.nih.gov/pubmed/16093540.

49. Peretti GM, Randolph MA, Zaporojan V, et al. 2001. A biomechanical analysis of an engineered cell-scaffold implant for cartilage repair. [Internet].Ann. Plast. Surg. 46(5):533–7[cited 2015 Feb 5] Available from: http://www.ncbi.nlm.nih.gov/pubmed/11352428.

50. Lee CR, Grodzinsky AJ, Hsu HP, et al. 2000. Effects of harvest and selected cartilage repair procedures on the physical and biochemical properties of articular cartilage in the canine knee. [Internet].J. Orthop. Res. 18(5):790–9[cited 2015 Feb 5] Available from: http://www.ncbi.nlm.nih.gov/pubmed/11117302.

51. Russlies M, Rüther P, Köller W, et al. [Biomechanical properties of cartilage repair tissue after different cartilage repair procedures in sheep]. [Internet].Z. Orthop. Ihre Grenzgeb. 141(4):465–71[cited 2015 Jan 30] Available from: http://www.ncbi.nlm.nih.gov/pubmed/12929006.

52. Jones CW, Willers C, Keogh A, et al. 2008. Matrix-induced autologous chondrocyte implantation in sheep: objective assessments including confocal arthroscopy. [Internet].J. Orthop. Res. 26(3):292–303[cited 2015 Feb 5] Available from: http://www.ncbi.nlm.nih.gov/pubmed/17902176.

53. Nixon AJ, Begum L, Mohammed HO, et al. 2011. Autologous chondrocyte implantation drives early chondrogenesis and organized repair in extensive full- and partial-thickness cartilage defects in an equine model. [Internet].J. Orthop. Res. 29(7):1121–30[cited 2015 Feb 5] Available from: http://www.ncbi.nlm.nih.gov/pubmed/21319216.

54. Gleghorn JP, Jones ARC, Flannery CR, Bonassar LJ. 2007. Boundary mode frictional properties of engineered cartilaginous tissues. [Internet].Eur. Cell.

Mater. 14:20–8; discussion 28–9[cited 2015 Feb 5] Available from: http://www.ncbi.nlm.nih.gov/pubmed/17676563.

55. Chang SC, Rowley JA, Tobias G, et al. 2001. Injection molding of chondrocyte/alginate constructs in the shape of facial implants. [Internet].J. Biomed. Mater. Res. 55(4):503–11[cited 2015 Feb 5] Available from: http://www.ncbi.nlm.nih.gov/pubmed/11288078.

56. Bonnevie ED, Puetzer JL, Bonassar LJ. 2014. Enhanced boundary lubrication properties of engineered menisci by lubricin localization with insulin-like growth factor I treatment. [Internet].J. Biomech. 47(9):2183–8[cited 2015 Feb 5] Available from: http://www.ncbi.nlm.nih.gov/pubmed/24210471.

57. Gleghorn JP, Doty SB, Warren RF, et al. 2010. Analysis of frictional behavior and changes in morphology resulting from cartilage articulation with porous polyurethane foams. [Internet].J. Orthop. Res. 28(10):1292–9[cited 2015 Feb 5] Available from: http://www.ncbi.nlm.nih.gov/pubmed/20309861.

58. Galley NK, Gleghorn JP, Rodeo S, et al. 2011. Frictional properties of the meniscus improve after scaffold-augmented repair of partial meniscectomy: a pilot study. [Internet].Clin. Orthop. Relat. Res. 469(10):2817–23[cited 2015 Feb 5] Available from: http://www.pubmedcentral.nih.gov/articlerender.fcgi?artid=3171552&tool=pmcentrez&rendertype=abstract.

59. Griffin DJ, Vicari J, Buckley MR, et al. 2014. Effects of enzymatic treatments on the depth-dependent viscoelastic shear properties of articular cartilage. [Internet].J. Orthop. Res. 32(12):1652–7[cited 2015 Jan 13] Available from: http://www.ncbi.nlm.nih.gov/pubmed/25196502.

60. Buckley MR, Bonassar LJ, Cohen I. 2012. Localization of Viscous Behavior and Shear Energy Dissipation in Articular Cartilage Under Dynamic Shear Loading [Internet].J. Biomech. Eng. 135(3):31002[cited 2014 Jan 30] Available from: http://www.ncbi.nlm.nih.gov/pubmed/24231813.

61. Silverberg JL, Dillavou S, Bonassar L, Cohen I. 2013. Anatomic variation of depth-dependent mechanical properties in neonatal bovine articular cartilage. [Internet].J. Orthop. Res. 31(5):686–91[cited 2014 Feb 12] Available from: http://www.ncbi.nlm.nih.gov/pubmed/23280608.

62. Buckley MR, Gleghorn JP, Bonassar LJ, Cohen I. 2008. Mapping the depth dependence of shear properties in articular cartilage. [Internet].J. Biomech. 41(11):2430–2437[cited 2014 Feb 7] Available from: http://www.ncbi.nlm.nih.gov/pubmed/18619596.

63. Buckley MR, Bergou AJ, Fouchard J, et al. 2010. High-resolution spatial mapping of shear properties in cartilage. [Internet].J. Biomech. 43(4):796–800[cited 2014 Feb 7] Available from: http://www.pubmedcentral.nih.gov/articlerender.fcgi?artid=2832609&tool=pmcentrez&rendertype=abstract.

64. Lane J, Healey R, Amiel D. 2009. Changes in condylar coefficient of friction after osteochondral graft transplantation and modulation with hyaluronan. [Internet].Arthroscopy 25(12):1401–7[cited 2015 Apr 2] Available from: http://www.sciencedirect.com/science/article/pii/S074980630900423X.

65. Neu CP, Komvopoulos K, Reddi AH. 2008. The interface of functional biotribology and regenerative medicine in synovial joints. [Internet].Tissue Eng. Part B. Rev. 14(3):235–47[cited 2015 Apr 2] Available from: http://www.pubmedcentral.nih.gov/articlerender.fcgi?artid=2761828&tool=pmcentrez&rendertype=abstract.

66. Grad S, Loparic M, Peter R, et al. 2012. Sliding motion modulates stiffness and friction coefficient at the surface of tissue engineered cartilage. [Internet].Osteoarthritis Cartilage 20(4):288–95[cited 2015 Jan 30] Available from: http://www.ncbi.nlm.nih.gov/pubmed/22285735.

67. Huang AH, Baker BM, Ateshian GA, Mauck RL. 2012. Sliding contact loading enhances the tensile properties of mesenchymal stem cell-seeded hydrogels. [Internet].Eur. Cell. Mater. 24:29–45[cited 2015 Feb 5] Available from: http://www.ncbi.nlm.nih.gov/pubmed/22791371.

68. Singh A, Corvelli M, Unterman SA, et al. 2014. Enhanced lubrication on tissue and biomaterial surfaces through peptide-mediated binding of hyaluronic acid. [Internet].Nat. Mater. 13(10):988–95[cited 2015 Apr 2] Available from: http://www.ncbi.nlm.nih.gov/pubmed/25087069.

69. Bhumiratana S, Eton RE, Oungoulian SR, et al. 2014. Large, stratified, and mechanically functional human cartilage grown in vitro by mesenchymal condensation. [Internet].Proc. Natl. Acad. Sci. U. S. A. 111(19):6940–5[cited 2015 Apr 2] Available from: http://www.pubmedcentral.nih.gov/articlerender.fcgi?artid=4024923&tool=pmcentrez&rendertype=abstract.

70. Palmer AW, Wilson CG, Baum EJ, Levenston ME. 2009. Composition-function relationships during IL-1-induced cartilage degradation and recovery. [Internet].Osteoarthritis Cartilage 17(8):1029–39[cited 2015 Apr 2] Available from: http://www.pubmedcentral.nih.gov/articlerender.fcgi?artid=2745941&tool=pmcentrez&rendertype=abstract.

71. Silverberg JL, Barrett AR, Das M, et al. 2014. Structure-function relations and rigidity percolation in the shear properties of articular cartilage. [Internet].Biophys. J. 107(7):1721–30[cited 2015 Feb 5] Available from: http://www.cell.com/article/S0006349514008546/fulltext.

72. Brittberg M, Lindahl A, Nilsson A, et al. 1994. Treatment of deep cartilage defects in the knee with autologous chondrocyte transplantation. [Internet].N. Engl. J. Med. 331(14):889–95[cited 2015 Mar 1] Available from: http://www.ncbi.nlm.nih.gov/pubmed/8078550.

73. Nixon AJ, Begum L, Mohammed HO, et al. 2011. Autologous chondrocyte implantation drives early chondrogenesis and organized repair in extensive full- and partial-thickness cartilage defects in an equine model. [Internet].J. Orthop. Res. 29(7):1121–30[cited 2015 Feb 5] Available from: http://www.ncbi.nlm.nih.gov/pubmed/21319216.

74. Bartlett W, Gooding CR, Carrington RWJ, et al. 2005. Autologous chondrocyte implantation at the knee using a bilayer collagen membrane with bone graft. A preliminary report. [Internet].J. Bone Joint Surg. Br. 87(3):330–2[cited 2015 Apr 20] Available from: http://www.ncbi.nlm.nih.gov/pubmed/15773640.

75. Kiess W, Haskell JF, Lee L, et al. 1987. An antibody that blocks insulin-like growth factor (IGF) binding to the type II IGF receptor is neither an agonist nor an inhibitor of IGF-stimulated biologic responses in L6 myoblasts. [Internet].J. Biol. Chem. 262(26):12745–51[cited 2015 May 13] Available from: http://www.ncbi.nlm.nih.gov/pubmed/2957378.

76. Madry H, Kaul G, Cucchiarini M, et al. 2005. Enhanced repair of articular cartilage defects in vivo by transplanted chondrocytes overexpressing insulin-like growth factor I (IGF-I). [Internet].Gene Ther. 12(15):1171–9[cited 2015 May 13] Available from: http://www.ncbi.nlm.nih.gov/pubmed/15815701.

77. Goodrich LR, Brower-Toland BD, Warnick L, et al. 2006. Direct adenovirus-mediated IGF-I gene transduction of synovium induces persisting synovial fluid IGF-I ligand elevations. [Internet].Gene Ther. 13(17):1253–62[cited 2015 May 13] Available from: http://www.ncbi.nlm.nih.gov/pubmed/16708081.

78. Goodrich LR, Hidaka C, Robbins PD, et al. 2007. Genetic modification of chondrocytes with insulin-like growth factor-1 enhances cartilage healing in an equine model. [Internet].J. Bone Joint Surg. Br. 89(5):672–85[cited 2015 Apr 20] Available from: http://www.ncbi.nlm.nih.gov/pubmed/17540757.

79. Griffin D, Bonnevie E, Lachowsky D, et al. 2015. Mechanical Characterization of Matrix-Induced Autologous Chondrocyte Implantation (MACI®) Grafts in an Equine Model at 53 weeks [Internet].J. Biomech. [cited 2015 Apr 18] Available from: http://www.sciencedirect.com/science/article/pii/S0021929015002262.

80. Gratz KR, Wong VW, Chen AC, et al. 2006. Biomechanical assessment of tissue retrieved after in vivo cartilage defect repair: tensile modulus of repair tissue and integration with host cartilage. [Internet].J. Biomech. 39(1):138–46[cited 2015 Apr 20] Available from: http://www.ncbi.nlm.nih.gov/pubmed/16271598.

81. Dresdale A, Rose EA, Jeevanandam V, et al. 1985. Preparation of fibrin glue from single-donor fresh-frozen plasma. [Internet].Surgery 97(6):750–5[cited 2015 Apr 20] Available from: http://www.ncbi.nlm.nih.gov/pubmed/3873716.

82. Ortved KF, Begum L, Mohammed HO, Nixon AJ. 2015. Implantation of rAAV5-IGF-I transduced autologous chondrocytes improves cartilage repair in full-thickness defects in the equine model. [Internet].Mol. Ther. 23(2):363–73[cited 2015 Apr 20] Available from: http://www.ncbi.nlm.nih.gov/pubmed/25311491.

83. Chang SC, Rowley JA, Tobias G, et al. 2001. Injection molding of chondrocyte/alginate constructs in the shape of facial implants. [Internet].J. Biomed. Mater. Res. 55(4):503–11[cited 2015 Feb 5] Available from: http://www.ncbi.nlm.nih.gov/pubmed/11288078.

84. Strauss EJ, Goodrich LR, Chen C-T, et al. 2005. Biochemical and biomechanical properties of lesion and adjacent articular cartilage after chondral defect repair in an equine model. [Internet].Am. J. Sports Med. 33(11):1647–53[cited 2015 Feb 5] Available from: http://www.ncbi.nlm.nih.gov/pubmed/16093540.

85. Poole AR. 2003. What type of cartilage repair are we attempting to attain? [Internet].J. Bone Joint Surg. Am. 85-A Suppl:40–4[cited 2015 May 6] Available from: http://www.ncbi.nlm.nih.gov/pubmed/12721344.

86. Russlies M, Rüther P, Köller W, et al. 2003. [Biomechanical properties of cartilage repair tissue after different cartilage repair procedures in sheep].

[Internet].Z. Orthop. Ihre Grenzgeb. 141(4):465–71[cited 2015 May 13] Available from: http://europepmc.org/abstract/med/12929006.

87. Maroudas AI. 1976. Balance between swelling pressure and collagen tension in normal and degenerate cartilage. [Internet].Nature 260(5554):808–9[cited 2015 May 13] Available from: http://www.ncbi.nlm.nih.gov/pubmed/1264261.

88. Gannon AR, Nagel T, Bell AP, et al. 2015. The changing role of the superficial region in determining the dynamic compressive properties of articular cartilage during postnatal development. [Internet].Osteoarthritis Cartilage [cited 2015 May 5] Available from: http://www.sciencedirect.com/science/article/pii/S1063458415000448.

89. Williamson AK, Chen AC, Sah RL. 2001. Compressive properties and function-composition relationships of developing bovine articular cartilage. [Internet].J. Orthop. Res. 19(6):1113–21[cited 2015 Apr 20] Available from: http://www.ncbi.nlm.nih.gov/pubmed/11781013.

90. Maroudas A. 2002. Physico-Chemical Properties Of Human Articular Cartilage [Internet].J. Bone Jt. Surgery, Br. Vol. 84-B(SUPP III):309–310[cited 2015 Apr 20] Available from: http://www.bjjprocs.boneandjoint.org.uk/content/84-B/SUPP_III/309.6.abstract.

91. Hangody L, Kárpáti Z. 1994. [New possibilities in the management of severe circumscribed cartilage damage in the knee]. [Internet].Magy. Traumatol. Ortop. Kezseb. Plasztikai Seb. 37(3):237–43[cited 2015 Nov 30] Available from: http://www.ncbi.nlm.nih.gov/pubmed/7920908.

92. Nehrer S, Spector M, Minas T. 1999. Histologic analysis of tissue after failed cartilage repair procedures. [Internet].Clin. Orthop. Relat. Res. (365):149–62[cited 2015 Apr 20] Available from: http://www.ncbi.nlm.nih.gov/pubmed/10627699.

93. Jackson DW, Lalor PA, Aberman HM, Simon TM. 2001. Spontaneous repair of full-thickness defects of articular cartilage in a goat model. A preliminary study. [Internet].J. Bone Joint Surg. Am. 83-A(1):53–64[cited 2015 Apr 20] Available from: http://www.ncbi.nlm.nih.gov/pubmed/11205859.

94. Hallal PC, Wells JCK, Bertoldi AD, et al. 2005. A shift in the epidemiology of low body mass index in Brazilian adults. [Internet].Eur. J. Clin. Nutr. 59(9):1002–6[cited 2015 Nov 30] Available from:

http://www.ncbi.nlm.nih.gov/pubmed/15970943.

95. Hangody L, Kish G, Kárpáti Z, et al. 1997. Arthroscopic autogenous osteochondral mosaicplasty for the treatment of femoral condylar articular defects. A preliminary report. [Internet].Knee Surg. Sports Traumatol. Arthrosc. 5(4):262–7[cited 2015 Apr 20] Available from: http://www.ncbi.nlm.nih.gov/pubmed/9430578.

96. Mow VC, Ratcliffe A, Rosenwasser MP, Buckwalter JA. 1991. Experimental studies on repair of large osteochondral defects at a high weight bearing area of the knee joint: a tissue engineering study. [Internet].J. Biomech. Eng. 113(2):198–207[cited 2015 Apr 24] Available from: http://www.ncbi.nlm.nih.gov/pubmed/1875694.

97. Peterson L, Brittberg M, Kiviranta I, et al. 2002. Autologous Chondrocyte Transplantation: Biomechanics and Long-Term Durability [Internet].Am. J. Sport. Med. 30(1):2–12[cited 2015 May 13] Available from: http://ajs.sagepub.com/content/30/1/2.short.

98. Henderson I, Lavigne P, Valenzuela H, Oakes B. 2007. Autologous chondrocyte implantation: superior biologic properties of hyaline cartilage repairs. [Internet].Clin. Orthop. Relat. Res. 455:253–61[cited 2015 Feb 5] Available from: http://www.ncbi.nlm.nih.gov/pubmed/16980901.

99. Peterson L, Brittberg M, Kiviranta I, et al. Autologous chondrocyte transplantation. Biomechanics and long-term durability. [Internet].Am. J. Sports Med. 30(1):2–12[cited 2015 Feb 5] Available from: http://www.ncbi.nlm.nih.gov/pubmed/11798989.

100. Griffin D, Bonnevie E, Lachowsky D, et al. 2015. Mechanical Characterization of Matrix-Induced Autologous Chondrocyte Implantation (MACI®) Grafts in an Equine Model at 53 weeks [Internet].J. Biomech. [cited 2015 Apr 18] Available from: http://www.sciencedirect.com/science/article/pii/S0021929015002262.

101. Chu CR, Dounchis JS, Yoshioka M, et al. 1997. Osteochondral repair using perichondrial cells. A 1-year study in rabbits. [Internet].Clin. Orthop. Relat. Res. (340):220–9[cited 2015 Apr 24] Available from: http://www.ncbi.nlm.nih.gov/pubmed/9224260.

102. Madry H, Kaul G, Zurakowski D, et al. 2013. Cartilage constructs engineered

from chondrocytes overexpressing IGF-I improve the repair of osteochondral defects in a rabbit model. [Internet].Eur. Cell. Mater. 25:229–47[cited 2015 May 13] Available from: http://www.ncbi.nlm.nih.gov/pubmed/23588785.

103. Reindel ES, Ayroso AM, Chen AC, et al. 1995. Integrative repair of articular cartilage in vitro: adhesive strength of the interface region. [Internet].J. Orthop. Res. 13(5):751–60[cited 2015 Apr 9] Available from: http://www.ncbi.nlm.nih.gov/pubmed/7472754.

104. DiMicco MA, Waters SN, Akeson WH, Sah RL. 2002. Integrative articular cartilage repair: dependence on developmental stage and collagen metabolism. [Internet].Osteoarthritis Cartilage 10(3):218–25[cited 2015 Apr 23] Available from: http://www.sciencedirect.com/science/article/pii/S1063458401905023.

105. Gratz KR, Wong VW, Chen AC, et al. 2006. Biomechanical assessment of tissue retrieved after in vivo cartilage defect repair: tensile modulus of repair tissue and integration with host cartilage. [Internet].J. Biomech. 39(1):138–46[cited 2015 Apr 20] Available from: http://www.jbiomech.com/article/S0021929004005330/fulltext.

106. van de Breevaart Bravenboer J, In der Maur CD, Bos PK, et al. 2004. Improved cartilage integration and interfacial strength after enzymatic treatment in a cartilage transplantation model. [Internet].Arthritis Res. Ther. 6(5):R469–76[cited 2015 Apr 23] Available from: http://arthritis-research.com/content/6/5/R469.

107. Obradovic B, Martin I, Padera RF, et al. 2001. Integration of engineered cartilage. [Internet].J. Orthop. Res. 19(6):1089–97[cited 2015 Apr 24] Available from: http://www.ncbi.nlm.nih.gov/pubmed/11781010.

108. Brittberg M, Lindahl A, Nilsson A, et al. 1994. Treatment of deep cartilage defects in the knee with autologous chondrocyte transplantation. [Internet].N. Engl. J. Med. 331(14):889–95[cited 2015 Mar 1] Available from: http://www.ncbi.nlm.nih.gov/pubmed/8078550.

109. Peretti GM, Bonassar LJ, Caruso EM, et al. 1999. Biomechanical analysis of a chondrocyte-based repair model of articular cartilage. [Internet].Tissue Eng. 5(4):317–26[cited 2015 Apr 24] Available from: http://www.ncbi.nlm.nih.gov/pubmed/10477854.

120. Buckley MR, Gleghorn JP, Bonassar LJ, Cohen I. 2008. Mapping the depth

dependence of shear properties in articular cartilage. [Internet].J. Biomech. 41(11):2430–2437[cited 2014 Feb 7] Available from: http://www.ncbi.nlm.nih.gov/pubmed/18619596.

121. Silverberg JL, Barrett AR, Das M, et al. 2014. Structure-function relations and rigidity percolation in the shear properties of articular cartilage. [Internet].Biophys. J. 107(7):1721–30[cited 2015 Feb 5] Available from: http://www.cell.com/article/S0006349514008546/fulltext.

122. Buckley MR, Bonassar LJ, Cohen I. 2012. Localization of Viscous Behavior and Shear Energy Dissipation in Articular Cartilage Under Dynamic Shear Loading [Internet].J. Biomech. Eng. 135(3):31002[cited 2014 Jan 30] Available from: http://www.ncbi.nlm.nih.gov/pubmed/24231813.

123. Griffin DJ, Vicari J, Buckley MR, et al. 2014. Effects of enzymatic treatments on the depth-dependent viscoelastic shear properties of articular cartilage. [Internet].J. Orthop. Res. 32(12):1652–7[cited 2015 Jan 13] Available from: http://www.ncbi.nlm.nih.gov/pubmed/25196502.

124. Silverberg JL, Dillavou S, Bonassar L, Cohen I. 2013. Anatomic variation of depth-dependent mechanical properties in neonatal bovine articular cartilage. [Internet].J. Orthop. Res. 31(5):686–91[cited 2014 Feb 12] Available from: http://www.ncbi.nlm.nih.gov/pubmed/23280608.

125. Michalek AJ, Buckley MR, Bonassar LJ, et al. 2009. Measurement of local strains in intervertebral disc anulus fibrosus tissue under dynamic shear: contributions of matrix fiber orientation and elastin content. [Internet].J. Biomech. 42(14):2279–2285[cited 2014 Jan 21] Available from: http://www.pubmedcentral.nih.gov/articlerender.fcgi?artid=2757465&tool=pmcentrez&rendertype=abstract.

126. Spangenberg KM, Peretti GM, Trahan CA, et al. 2002. Histomorphometric analysis of a cell-based model of cartilage repair. [Internet].Tissue Eng. 8(5):839–46[cited 2015 Dec 7] Available from: http://online.liebertpub.com/doi/abs/10.1089/10763270260424196.

127. Peretti GM, Zaporojan V, Spangenberg KM, et al. 2003. Cell-based bonding of articular cartilage: An extended study. [Internet].J. Biomed. Mater. Res. A 64(3):517–24[cited 2015 Dec 7] Available from: http://www.ncbi.nlm.nih.gov/pubmed/12579566.

128. Fortier LA, Mohammed HO, Lust G, Nixon AJ. 2002. Insulin-like growth factor-I enhances cell-based repair of articular cartilage. [Internet].J. Bone Joint Surg. Br. 84(2):276–88[cited 2015 Apr 23] Available from: http://www.ncbi.nlm.nih.gov/pubmed/11922373.

129. Strauss EJ, Goodrich LR, Chen C-T, et al. 2005. Biochemical and biomechanical properties of lesion and adjacent articular cartilage after chondral defect repair in an equine model. [Internet].Am. J. Sports Med. 33(11):1647–53[cited 2015 Feb 5] Available from: http://www.ncbi.nlm.nih.gov/pubmed/16093540.

130. Ortved KF, Begum L, Mohammed HO, Nixon AJ. 2015. Implantation of rAAV5-IGF-I transduced autologous chondrocytes improves cartilage repair in full-thickness defects in the equine model. [Internet].Mol. Ther. 23(2):363–73[cited 2015 Apr 20] Available from: http://www.ncbi.nlm.nih.gov/pubmed/25311491.

131. Proffen BL, Sieker JT, Murray MM, et al. 2015. Extracellular matrix-blood composite injection reduces post-traumatic osteoarthritis after anterior cruciate ligament injury in the rat. [Internet].J. Orthop. Res. [cited 2015 Dec 9] Available from: http://www.ncbi.nlm.nih.gov/pubmed/26629963.

132. Faschingbauer M, Renner L, Waldstein W, Boettner F. 2015. Are lateral compartment osteophytes a predictor for lateral cartilage damage in varus osteoarthritic knees? : Data from the Osteoarthritis Initiative. [Internet].Bone Joint J. 97-B(12):1634–9[cited 2015 Dec 9] Available from: http://www.ncbi.nlm.nih.gov/pubmed/26637677.

133. Gratz KR, Wong VW, Chen AC, et al. 2006. Biomechanical assessment of tissue retrieved after in vivo cartilage defect repair: tensile modulus of repair tissue and integration with host cartilage. [Internet].J. Biomech. 39(1):138–46[cited 2015 Apr 20] Available from: http://www.ncbi.nlm.nih.gov/pubmed/16271598.

134. Fujie H, Nansai R, Ando W, et al. 2015. Zone-specific integrated cartilage repair using a scaffold-free tissue engineered construct derived from allogenic synovial mesenchymal stem cells: Biomechanical and histological assessments. [Internet].J. Biomech. 48(15):4101–8[cited 2015 Nov 19] Available from: http://www.ncbi.nlm.nih.gov/pubmed/26549765.

135. Malda J, Kreijveld E, Temenoff JS, et al. 2003. Expansion of human nasal chondrocytes on macroporous microcarriers enhances redifferentiation. [Internet].Biomaterials 24(28):5153–61[cited 2015 Dec 14] Available from: http://www.ncbi.nlm.nih.gov/pubmed/14568432.